Oncolytic viral therapies and the delicate balance between virus-macrophage-tumour interactions

Almuallem, Nada; Trucu, Dumitru; Eftimie, Raluca

Published in:
Mathematical Biosciences and Engineering

DOI:
10.3934/mbe.2021041

Publication date:
2021

Mathematical Biosciences and Engineering

http://www.aimspress.com/journal/MBE

MBE, 18(1): 764–799.
DOI: 10.3934/mbe.2021041
Received: 18 October 2020
Accepted: 06 December 2020
Published: 18 December 2020

Research article

Oncolytic viral therapies and the delicate balance between virus-macrophage-tumour interactions: A mathematical approach

Nada Almuallem, Dumitru Trucu and Raluca Eftimie*

Department of Mathematics, University of Dundee, Dundee, DD1 4HN, UK

* **Correspondence:** r.a.eftimie@dundee.ac.uk; Tel: +44 (0)1382 384488.

Abstract: The success of oncolytic virotherapies depends on the tumour microenvironment, which contains a large number of infiltrating immune cells. In this theoretical study, we derive an ODE model to investigate the interactions between breast cancer tumour cells, an oncolytic virus (Vesicular Stomatitis Virus), and tumour-infiltrating macrophages with different phenotypes which can impact the dynamics of oncolytic viruses. The complexity of the model requires a combined analytical-numerical approach to understand the transient and asymptotic dynamics of this model. We use this model to propose new biological hypotheses regarding the impact on tumour elimination/relapse/persistence of: (i) different macrophage polarisation/re-polarisation rates; (ii) different infection rates of macrophages and tumour cells with the oncolytic virus; (iii) different viral burst sizes for macrophages and tumour cells. We show that increasing the rate at which the oncolytic virus infects the tumour cells can delay tumour relapse and even eliminate tumour. Increasing the rate at which the oncolytic virus particles infect the macrophages can trigger transitions between steady-state dynamics and oscillatory dynamics, but it does not lead to tumour elimination unless the tumour infection rate is also very large. Moreover, we confirm numerically that a large tumour-induced M1→M2 polarisation leads to fast tumour growth and fast relapse (if the tumour was reduced before by a strong anti-tumour immune and viral response). The increase in viral-induced M2→M1 re-polarisation reduces temporarily the tumour size, but does not lead to tumour elimination. Finally, we show numerically that the tumour size is more sensitive to the production of viruses by the infected macrophages.

Keywords: mathematical model; Vesicular Stomatitis Virus (VSV); breast cancer cells; M1 macrophages; M2 macrophages; asymptotic dynamics

1. Introduction

Oncolytic viral therapies have become one of the most promising therapies for cancer, due to the ability of some viruses (i.e., oncolytic viruses) to replicate inside tumour cells without damaging

normal tissue cells [50]. In addition to their ability to selectively replicate inside cancer cells, which leads to the destruction of these cells, oncolytic viruses can also trigger anti-tumour immune responses [34]. However, these anti-tumour immune responses are counterbalanced by anti-viral immune responses which eliminate the virus particles from the body [14]. Therefore, the success of these oncolytic therapies depends on a better understanding of the interactions between immune cells (and in particular cells of innate immunity) and oncolytic viruses.

Macrophages represent the first line of defence against pathogens, and they have been shown to eliminate viruses in an interferon-dependent manner [40, 50, 52]. However, macrophages can also be infected by viruses, and thus enhance viral dissemination and persistence [37]. The different roles of macrophages on virus elimination and/or persistence might be explained by the heterogeneity of macrophage population. These immune cells can have a variety of polarisation phenotypes, depending on the microenvironment they are in, and on the activation stimuli. The two extreme macrophage phenotypes are represented by the classically-activated anti-tumour and anti-viral M1 cells, and the alternatively-activated pro-tumour and anti-inflammatory M2 cells [31,49]. The M1-like macrophages have been shown to produce anti-viral interferons [49, 55]. While many viral pathogens have been shown to activate a M1 polarisation, some viruses benefit from skewing macrophages towards an M2-like phenotype [38]. The M2-like macrophages seem to act as reservoirs of replication for many viruses: from the human immunodeficiency virus (HIV) to the human cytomegalovirus (HCMV) [38]. Recent studies have shown that a promising oncolytic virus, the Vesicular Stomatitis Virus (VSV), can infect and replicate inside M2 cells but not inside M1 cells [60].

In addition to macrophages importance in anti-viral immune responses, these innate immune cells have also been found to infiltrate many types of solid tumours, and can represent between 5%–50% of tumour mass [69, 73]. The tumour-associated macrophages usually have a M2-like phenotype, as tumour cells educate macrophages towards a phenotype that supports their growth. Since these tumour-associated M2-like cells can be infected by some oncolytic viruses [60, 61], a better understanding of the interactions between M1 cells, M2 cells, oncolytic viruses and tumour cells is necessary to improve current treatment approaches [15].

In this theoretical study we focus on one of the most promising oncolytic viruses currently undergoing research, the oncolytic Vesicular Stomatitis Virus (VSV), which naturally infects and replicates inside cancer cells with defects in their antiviral responses (e.g., defects in the IFNγ pathway) [1]. Very recently, this oncolytic virus has been shown to replicate inside M2 macrophages but not inside M1 macrophages [60]. Moreover, the VSV seems to re-program the pro-tumour M2 macrophages towards the anti-tumour M1 phenotype [60], and this re-programming is triggered by the activation of the type-I IFN anti-viral response [58]. In regard to the cancer cell line, the experiments in [25] on VSV-macrophages-cancer interactions focused on a breast cancer cell line: MDA-MB-231. In [30] it was shown that this MDA-MB-131 cell line activates macrophages towards an M2 phenotype. Moreover, this particular cancer cell line is infiltrated by large numbers of macrophages [44]. For all these reasons, in this theoretical study we decided to focus on the same cancer cell line: the MDA-MB-231 cells.

The main goal of this study is to derive and investigate a mathematical model that could help us better understand the complex interactions between macrophages and oncolytic viruses that lead to the elimination/growth of tumours, by tacking into account also the infection of macrophages with oncolytic virus particles. To this end we generalises the model in [4] (which focused only on

macrophage-virus interactions) by incorporating also tumour interactions with viruses and with M1 and M2 macrophages. To emphasise the novelty of our model, we note that the majority of mathematical models in the literature focus only on the interactions between tumour cells, oncolytic viruses and anti-tumour/anti-viral immune cells; see for example, [17, 19, 21, 32, 33, 36, 41, 46, 48] and references therein. Only a very small number of recent mathematical models investigate the infection of macrophages with oncolytic viruses, which can lead to the delivery of these viruses to specific areas of the tumour (e.g. necrotic region) [6].

Given the complexity of the new mathematical model that we propose in this study, it is impossible to focus exclusively on analytical results. Thus, here we combine some analytical results such as the identification of steady states and their linear stability analysis, with computational results, to gain a better understanding of overall model dynamics (e.g., the correlations between different model steady states that cannot be calculated analytically; the changes in these complex steady states as we vary model parameters). We also consider computational approaches to answer the following biological questions:

(i) What could be the effect of macrophage polarisation/re-polarisation on tumour-oncolytic virus dynamics?
(ii) What could be the effect of VSV infection of M2 cells vs. infection of tumour cells on overall tumour growth/decay?
(iii) What could be the effect of VSV replication inside macrophages vs. replication inside tumour cells on overall tumour growth/decay?

Note that the last two questions refer to slightly different aspects of viral cycle: virus entry into the cells (i.e., infection rate, which can be reduced due to physical barriers inside solid tumours) and virus proliferation inside the cells which culminates with cell burst and the release of new virus particles.

The paper is structured as follows. Section 2 focuses on the description of a mathematical models for the interactions between tumour cells, M1 and M2 macrophages and oncolytic VSV particles. In section 3 we present some numerical results for the baseline dynamics of this model, as well model dynamics when we vary the infection rates of macrophages and tumour cells with the VSV particles, as well as the tumour-induced macrophage polarisation rate. We also investigate analytically the steady states and their stability (to get a better understanding of the long-term behaviour of this model), and use numerical approaches to shed some light on the analytical results that are difficult to obtain. We conclude with a summary and discussion in section 4.

2. Model description

To investigate the innate immune responses generated by macrophages roles on the anti-tumour oncolytic viral therapies (with VSV), we extend the mathematical model derived in [4], by considering the presence of a tumour population. Thus we focus on the following interacting cell populations: the density of uninfected tumour cells (T_u), the density of virus-infected tumour cells (T_i), the density of virions (V), the density of M_1 macrophages (which are resistant to VSV infection [61]), the densities of uninfected M_2 macrophages (M_{2u}) and the VSV-infected M2 macrophages (M_{2i}) [61]); see also

Figure 1. The time evolution of these variables is described by the following equations:

$$\frac{dT_u}{dt} = \underbrace{rT_u\left(1-\frac{T_u}{K_1}\right)}_{\text{logistic growth}} - \underbrace{\beta_1 V T_u}_{\text{tumour infection with VSV}} - \underbrace{d_u T_u \frac{M_1}{h_m + M_{2u}}}_{\text{tumour elimination by M1}} + \underbrace{d_m T_u \frac{M_{2u}}{h_m + M_{2u}}}_{\text{tumour promotion by M2u}}, \tag{2.1a}$$

$$\frac{dT_i}{dt} = \underbrace{\beta_1 V T_u}_{\text{tumour infection with VSV}} - \underbrace{\delta_{i1} T_i}_{\text{lysis by viruses}} - \underbrace{d_i T_i \frac{M_1}{h_m + M_{2u}}}_{\text{elimination of infected tumour by M1}}, \tag{2.1b}$$

$$\frac{dM_1}{dt} = \underbrace{a_1^v V + a_1^i T_i + a_1^u T_u}_{\text{activation of M1}} + \underbrace{p_{m1} M_1\left(1-\frac{M_1+M_{2u}}{K_2}\right)}_{\text{logistic growth}} - \underbrace{d_{e1} M_1}_{\text{natural death}} - \underbrace{M_1\left(r_{m1}^0 + r_{m1}^u \frac{T_u}{h_u+T_u}\right)}_{\text{M1}\to\text{M2 polarisation}} + \underbrace{M_{2u}\left(r_{m2}^0 + r_{m2}^v \frac{V}{h_v+V}\right)}_{\text{M2}\to\text{M1 re-polarisation}}, \tag{2.1c}$$

$$\frac{dM_{2u}}{dt} = \underbrace{a_2^u T_u}_{\text{activation of M2u}} + \underbrace{p_{m2} M_{2u}\left(1-\frac{M_1+M_{2u}}{K_2}\right)}_{\text{logistic growth}} + \underbrace{M_1\left(r_{m1}^0 + r_{m1}^u \frac{T_u}{h_u+T_u}\right)}_{\text{M1}\to\text{M2 polarisation}} - \underbrace{d_{e2} M_{2u}}_{\text{natural death}} - \underbrace{M_{2u}\left(r_{m2}^0 + r_{m2}^v \frac{V}{h_v+V}\right)}_{\text{M2}\to\text{M1 re-polarisation}} - \underbrace{\beta_2 V M_{2u}}_{\text{M2 infection with VSV}}, \tag{2.1d}$$

$$\frac{dM_{2i}}{dt} = \underbrace{\beta_2 V M_{2u}}_{\text{M2 infection with VSV}} - \underbrace{\delta_{i2} M_{2i}}_{\text{lysis by viruses}}, \tag{2.1e}$$

$$\frac{dV}{dt} = \underbrace{b\,\delta_{i1} T_i + c\,\delta_{i2} M_{2i}}_{\text{production of viruses}} - \underbrace{\omega V}_{\text{natural death}} - \underbrace{\delta_v V \frac{M_1}{h_m + M_{2u}}}_{\text{elimination of viruses by M1}}. \tag{2.1f}$$

Equations (2.1a)–(2.1f) incorporate the following biological mechanisms:

- The uninfected tumour cells (see Eq (2.1a)), grow at a rate r up to a carrying capacity K_1. We choose logistic growth since experimental studies have shown that tumour growth slows down as the tumour becomes very large and it depletes the nutrients [29, 39]. We assume that the virus particles can infect the tumour cells at a rate β_1, and the infection term is bilinear (i.e., the infection rate per virus and per uninfected cell is constant; for similar assumptions see [56,57,59,77]). The uninfected tumour cells can be eliminated by M1 macrophages at a rate d_u [79]. At the same time, the anti-tumour immune response generated by these M1 cells can be inhibited by the presence of M2 macrophages [67]. Finally, tumour proliferation can be enhanced, at a rate d_m, by the presence of M2 macrophages in the tumour microenvironment [2].
- The infected tumour cells (see Eq (2.1b)) are lysed at rate δ_{i1} following viral replication and cell burst. As for the uninfected cells, we assume that these infected cells can be eliminated by the M1

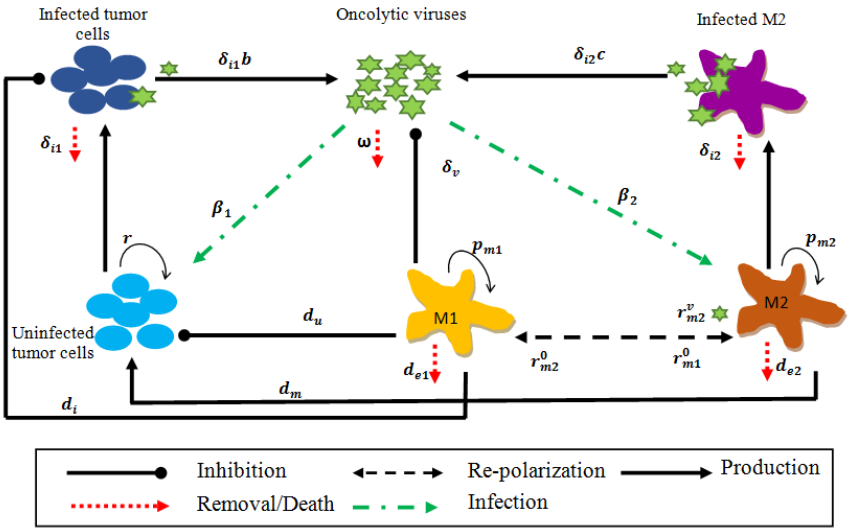

Figure 1. Graphical description of the possible non-spatial interactions between the tumour cells, oncolytic viruses and M1/M2 macrophages, as given by Eqs (2.1a)–(2.1f). The model was inspired by the experimental studies in [25, 45, 62], which showed that the VSV infects macrophages (but only the M2 cells, and not the M1 cells) in addition to the tumour cells, and the mathematical modelling studies in [18, 19], which focused only on the anti-viral effect of M1 cells and did not consider the infection of macrophages.

macrophages at a rate d_i. Again, we assume that the presence of M2 cells can inhibit the anti-viral effect of M1 cells [66].

- The M1 macrophages (see Eq (2.1c)), are activated by uninfected tumour cells at a rate a_1^u, by viral antigens at a rate a_1^v and by virus-infected tumour cells at a rate a_1^i. We assume that the M1 cells can proliferate logistically at a rate p_{m1} through a self renewal process [31], up to a maximum carrying capacity K_2. This type of growth depicts experimentally observed cell kinetics [11]. The M1 cells (which resist to VSV infections [61]) can polarise towards a M2 phenotype at a very small constant rate r_{m1}^0 (in response to cytokines such as IL-4, IL-10 [3] that can be produced by different healthy and immune cells in the microenvironment). We also assume that the presence of the tumour leads to an enhanced M1→M2 polarisation at a rate r_{m1}^u (since tumour cells produce large amounts of TGF-β, which is known to induce a M2 polarisation [27]). The M2→M1 re-polarisation of macrophages is assumed to occur at a very small constant rate r_{m2}^0 due to cytokines such as IFN-γ, IL-2 [3] produced by different types of healthy and immune cells in the environment. Moreover, it has been experimentally shown in [25] that matrix (M) protein mutant (rM51R-M) VSV could modulate the switch M2→M1 (probably through the induction of IFN-γ response [58]). Furthermore, engineering oncolytic viruses which carry specific cytokines can trigger a macrophages re-polarisation to a M1-like phenotype [28]. Thus, we assume that this enhanced M2→M1 re-polarisation occurs at a rate r_{m2}^v in the presence of the virus. The re-polarisation of M2 cells upon contact with VSV particles is described by a Michaelis-Menten term with constant h_v to account for the saturated re-polarising response induced by viruses. Finally, the M1 macrophages have a natural mortality rate d_{e1}.

- The uninfected M2 macrophages (see Eq (2.1d)) are activated at a rate a_2^u by the tumour cells, proliferate logistically at a rate p_{m2}, and have a natural mortality rate d_{e2}. The M1→M2 and M2→M1 polarisation terms have been described above. Finally, the M2 macrophages are predisposed to infections with VSV particles at a rate β_2 [61].
- The infected M2 macrophages (see Eq (2.1e)) are lysed by the replicating viruses at a rate δ_{i2}. All other terms have been described above.
- The oncolytic virus population (see Eq (2.1f)) proliferates when new virus particles are released by infected M2 cells and tumour cells. Parameters b and c describe the number of virus particles released by one infected tumour cell and one infected M2 macrophage, respectively. Moreover, the reduction in the number of virus particles is the result of their elimination, at a rate δ_v, by the M1 macrophages. Note that, as discussed in [15], viral clearance may be prevented by the M2 macrophages. Finally, we assume that the virus particles have a natural death rate ω [16]. This last term includes also the virus elimination rate by other innate immune cells (e.g., NK cells [74]) or adaptive immune cells (e.g., T cells [12]) not considered in this study.

Remark 1. *Because many experimental studies on the proliferation rates of macrophages do not distinguish between the M1 and M2 cells [11], throughout most of this study we will assume that* $p_{m1} = p_{m2} =: p_m$.

Remark 2. *Many modelling studies have included infected tumour cells in the carrying capacity terms (see [35,48]). Since in our study we did not see any significant changes in the model dynamics when we considered the infected cells (see Figure 14 in Appendix B we have decided to ignore the infected cells in the carrying capacity terms for both tumour and macrophages (see Eqs (2.1a), (2.1c) and (2.1d)).*

In the next sub-section we discuss in more detail the parameter values that we use to parametrise model (2.1).

2.1. Parameter values

In Table 1, we summarise the parameter values used throughout this theoretical study. Column 3 in Table 1 shows the dimensional values of the parameters (with units in column 4) – as obtained from the published literature (see discussion below) or estimated values/ranges. However, to avoid numerical problems caused by very large parameter values (see K_1, K_2 in column 3 in Table 1) and very small parameter values (see β_1, β_2 in column 3 in Table 1), we decided to rescale the cell populations by their carrying capacities (see also Appendix A): $T_u^* = T_u/K_1$, $T_i^* = T_i/K_1$, $M_1^* = M_1/K_2$, $M_{2u}^* = M_{2u}/K_2$, $M_{2i}^* = M_{2i}/K_2$. In addition, we rescaled the total virus population by $V_{max} = 10^{11}$, which is assumed to be the maximum viral load that does not cause neurotoxicity (see also Appendix A): $V^* = V/V_{max}$. This rescaling of variables leads to a rescaling of 11 parameters: $\beta_1, \beta_1, b, c, a_1^v, a_1^i, a_1^u, a_2^u, h_u, h_v, h_m$. These rescaled parameter values are listed in column 5 of Table 1. Note that for those parameter values that were not rescaled, columns 3 and 5 in Table 1 are identical.

Below we discuss the parameter values we approximated using experimental studies, and the values taken from the literature (especially if different mathematical studies used different parameter values).

- In this study we focus on the MDA-MB-231 tumour cell line, used to study late-stage breast cancer as it is invasive in vitro and metastasises spontaneously. For humane reasons, many *in-vivo* murine studies on tumour growth stop the murine experiments when tumours reach ≈ 1 cm^3

= 1000 mm^3 [71]. We can assume that at this size the tumour has likely depleted the organism of nutrients (so the tumour has reached its carrying capacity). Moreover, based on the study in [24] we assume that 1cm^3 tumour tissue contains maximum 10^9 tumour cells. Thus, for this study we choose a tumour carrying capacity of $K_1 = 10^9$ cells/cm^3.

- The doubling time of MDA-MB-231 cells varies depending on the culture medium. For example, Risinger et al. [64] calculated an average doubling time for MDA-MB-231 cells of 31.1 hr. Brown et al. [8] calculated a population doubling time between 1.05±0.091 days and 1.31±0.11 days on average. Corbin et al. [13] calculated an average cell doubling time around 26.7±8.8 hr. In this study we consider a tumour proliferation rate $r \in (0.47, 0.93)$, with an average of $r = 0.62$.
- In [22] the authors suggested that the doubling time of macrophages is around 27 hrs. In [81] the authors estimated the doubling time of untreated murine macrophage-like RAW264.7 cells to be between 18–22 hrs, while cells stimulated with bacterial lipopolysaccharide (LPS) had an estimated doubling time of 35 hrs. In [72], the authors estimated that M1 macrophages have a doubling time between 23.86 hrs and 28.97 hrs. In [11] it has been indicated that the average doubling time of macrophages is between 20–30 hrs. Therefore, from all these experimental studies we deduce that the doubling time of macrophages is likely between 18–35 hrs, which corresponds to proliferation rates between 0.4–0.9/day. For simplicity, through this study we choose the baseline proliferation rates $p_{m1} = p_{m2} = 0.57$/day, although we varied these rates within the interval $(0.4, 0.9)$.
- In regard to the M1/M2 macrophages natural death rates, various modelling studies used different values. For example, in [20] it was assumed that $d_{e1} = d_{e2} = 0.02$/day, the same as in [47]. On the other hand, in [18] the authors considered $d_{e1} = d_{e2} = 0.2$/day, as approximated from the experimental study in [78]. A recent experimental paper [31] suggested that the half-life of M1 pro-inflammatory murine M1 macrophages is between 18–20 hr (corresponding to a death rate between ln(2.0)/20hr and ln(2.0)/18hr), while the half-life of anti-inflammatory murine M2 cells is between 5–7 days (corresponding to a death rate between ln(2.0)/7days and ln(2.0)/5days). Therefore, for this study we choose $d_{e1} \in (0.83, 0.93)$ and $d_{e2} \in (0.099, 0.138)$.
- It is known that in breast cancer, up to 40% tumour size can be represented by macrophages [69]. Therefore, throughout this study we assume that the carrying capacity for macrophages is $K_2 = 40\%K_1 = 4 \times 10^8$.
- In regard to the lysis rate of infected macrophages, Rager *et. al* [63] showed that two macrophages cell lines (clones J774.16 and C3C, derived from the murine reticulum cell sarcoma J774) were completely lysed by the virus within 1–2 days after infection. Thus, in this study we assume a death rate of $\delta_{i2} \in \left(\frac{\ln(2.0)}{2}, \frac{\ln(2.0)}{1}\right) = (0.35, 0.69)$/day. For the simulations we use an average value of $\delta_{i2} = 0.52$.
- In regard to the VSV burst size, [63] showed that each productively infected macrophage was able to produce viral progeny of at least 1000PFU. Moreover, Zhu *et. al* [80] showed that each virus-infected tumour cell produced between 50 to 8000 progeny virus particles. For our numerical simulations we assume that the average burst size of infected tumour cells is $b = 2500$, which is the same value as in [18]. For the burst size of infected macrophages we assume $c = 2000$.
- The VSV death rate varies between different mathematical studies: e.g., $\omega = 2$/day in [18,46]), or $\omega \in (1 - 2.56)$/day in [21]. This is because experimental studies have shown that the intracellular half-lives of non-replicating wild type and mutant strains of VSV can vary between 5.3 hrs and

18 hrs, which translates into a death rate between ln(2)/5.3hr = 3.13 days and ln(2)/18hr= 0.92 days [16]. In [26] the authors have calculated the half-life of a replicating VSV strain between 2–15.9 hrs, which translates into a death rate between 1.04–8.31/day. In this study, we choose an average death rate of $\omega = 2$/day.

- In regard to the M1→M2 and M2→M1 baseline polarisation rates, the theoretical studies in [20, 75] used $r^0_{m1} \in (0.05, 0.09)$ and $r^0_{m2} \in (0.05, 0.08)$. In [18] the authors used the baseline values of $r^0_{m1} = 0.001$ and $r^0_{m2} = 0.01$. Here, we assume that these two parameters vary between $(10^{-5}, 10^{-1})$.
- For the virus-induced re-polarisation rate r^2_{m2} we used the same values as in [18], and thus we consider the baseline value $r^v_{m2} = 0$ (meaning that by default there is no virus-induced re-polarisation).
- The rest of the parameter values (i.e., h_m, h_v, δ_{i1}, β_1, β_2, δ_v, r^u_{m1}, g_2) used in this study for the numerical simulations are listed in Table 1. The ranges of these parameters, as well as their baseline values are "guessed", since we could not find any references for these parameters.
  To investigate the impact of these guessed parameters on the dynamics of uninfected tumour cells (T_u), we perform a global sensitivity analysis using the Latin Hypercube Sampling/Partial Rank Correlation Coefficient (PRCC) approach [5, 51]. In Figure 2 we plot the PRCC index for each model parameter, and we see that among these guessed parameter values only β_1 and r^u_{m1} have an impact on uninfected tumour cells T_u (since $\beta_1 \approx -0.8$, and $r^u_{m1} \approx -0.4$). Here we simulated tumour dynamics for 14 days; simulating tumour dynamics for longer time (e.g., 60–80 days) reduces the impact of r^u_{m1}; but β_1 still has an important role on tumour dynamics. In a similar manner we can investigate the sensitivity of M1 and M2 macrophages to model parameters; see Figures 15 and 16 in Appendix E. Both uninfected macrophage populations (M_1 and M_2) are most sensitive to two guessed parameters, h_u and r^v_{m2} (whose upper range is also guessed in Table 1).

Remark 3. *The study in [24] suggested that the detection level for human tumours is between* $10^7 - 10^9$ *cells. We can assume that for* in vivo *murine experiments, the detection level is between* $10^6 - 10^7$ *cells (since we are expecting to see tumour growth at the injection site). After the rescaling cell variables – see Appendix A – we assume that the detection level for the new rescaled tumours will be between* $10^{-3} - 10^{-2}$. *We will use this information in our discussion of numerical results.*

3. Results: steady states and their stability

We start investigating the dynamics of model (2.1) by focusing first on the long-term (asymptotic) behaviour of this model, i.e., the steady states and their stability. Due to the complexity of model (2.1), we combine analytical results with numerical simulations to gain a better understanding of this long-term dynamics. These steady-state results will be further used in section 3.2, where we will investigate numerically the transient and asymptotic behaviour of model (2.1), to explain the oscillatory and chaotic dynamics observed numerically in this model.

3.1. Steady states and their stability

Steady states. In this section we investigate the long-term behaviour of the model (2.1) by discussing all possible steady states. This steady-state investigation will allow us to understand better

Table 1. Summary of the parameters that appear in model (2.1), together with the original values and their units (columns 3, 4) and rescaled values (column 5) - used for the numerical simulations; for this rescaling, see Appendix A. The parentheses in columns 3 & 5 show the baseline values used for numerical simulations. The units are: "cells/vol" = "cells/mm^3" (for tumour, macrophages), and "PFU/vol" = plaque-forming units per vol (for VSV). Time is measured in "days".

Param.	Description & References	Values	Units	Rescaled Values
r	proliferation rate of tumour cells [8, 13, 64]	0.47 – 0.93 (0.62)	day^{-1}	0.47-0.93 (0.62)
K_1	carrying capacity of the tumour [24, 71]	10^9	$\frac{\text{cells}}{\text{vol}}$	1
g_1	coefficient that measures the contribution of infected tumour cells to tumour carrying capacity	0, 1	–	0, 1
β_1	infection rate of tumour cells with the oncolytic viruses (guessed value)	10^{-11} – 10^{-8} (10^{-9})	$\frac{\text{vol}}{\text{PFU}\times\text{day}}$	1 – 10^3 (10)
d_u	elimination rate of uninfected tumour cells by M1 macrophages [18]	10^{-2} – 10^1 (1)	day^{-1}	10^{-2} – 10^1 (1)
d_m	enhanced growth rate of uninfected tumour cells in the presence M2 macrophages [18]	10^{-2} – 10^1 (0.2)	day^{-1}	10^{-2} – 10^1 (0.2)
δ_{i1}	death rate of infected tumour cells due to viral lysis (guessed value)	0.3 – 0.7 (0.4)	days^{-1}	0.3 – 0.7 (0.4)
d_i	elimination rate of infected tumour cells by M1 macrophages [18]	10^{-1} – 10^1 (2)	day^{-1}	10^{-1} – 10^1 (2)
a_1^v	activation rate of M1 macrophages by viral antigens from VSV particles [18]	10^{-6} – 10^{-3} (10^{-4})	$\frac{\text{cells}}{\text{day}\times\text{PFU}}$	0.00025 – 0.25 (0.025)
a_1^i	activation rate of M1 macrophages by viral antigens from infected tumour cells [18]	10^{-6} – 10^{-3} (10^{-4})	day^{-1}	2.5×10^{-6}– 2.5×10^{-3} (0.00025)
a_1^u	activation rate of M1 macrophages in response to tumour antigen [18]	10^{-8} – 10^{-6} (5×10^{-8})	day^{-1}	2.5×10^{-8}– 2.5×10^{-6} (1.25×10^{-7})
p_{m1}	proliferation rate of M1 cells [11]	0.4 – 0.9 (0.57)	day^{-1}	0.4 – 0.9 (0.57)
r_{m1}^0	baseline M1→M2 re-polarisation rate in response to anti-inflammatory cytokines in the microenvironment [18]	10^{-5} – 10^{-1} (10^{-3})	day^{-1}	10^{-5} – 10^{-1} (10^{-3})
r_{m2}^0	baseline M2→M1 re-polarisation rate in response to pro-inflammatory cytokines in the microenvironment [18]	10^{-5} – 10^{-1} (10^{-3})	day^{-1}	10^{-5} – 10^{-1} (10^{-3})
r_{m1}^u	tumour-induced M1→M2 polarisation rate (guessed value)	0 – 10 (1)	day^{-1}	0 – 10 (1)
r_{m2}^v	VSV-induced M2→M1 re-polarisation rate [18]	0 – 10^1 (0)	day^{-1}	0 – 10^1 (0)
d_{e1}	natural death rate of M1 macrophages [31]	0.83 – 0.93 (0.88)	day^{-1}	0.83 – 0.93 (0.88)
d_{e2}	natural death rate of M2 macrophages [31]	0.099 – 0.138 (0.12)	day^{-1}	0.099 – 0.138 (0.12)
a_2^u	activation rate of M2 macrophages in response to tumour growth [18]	10^{-8} – 10^{-6} (10^{-7})	days^{-1}	2.5×10^{-8}– 2.5×10^{-6} (2.5×10^{-7})
p_{m2}	proliferation rate of M2 cells [11]	0.4 – 0.9 (0.57)	day^{-1}	0.4 – 0.9 (0.57)
K_2	carrying capacity of macrophages [69, 71]	4×10^8	cells/vol	1
g_2	coefficient that measures the contribution of infected tumour cells to tumour carrying capacity	0, 1	–	0, 1
β_2	infection rate of M2 macrophages with the oncolytic virus (guessed value)	10^{-11} – 10^{-8} (5×10^{-9})	$\frac{\text{vol}}{\text{PFU}\times\text{day}}$	1 – 10^3 (500)
δ_{i2}	rate at which an infected M2 cell is killed by the oncolytic virus particles [63]	0.35 – 0.69 (0.52)	day^{-1}	0.35 – 0.69 (0.52)
b	number of virus particles released from an infected tumour cell [80]	50 – 8000 (2500)	$\frac{\text{PFU}}{\text{cells}}$	0.5 – 80 (25)
c	number of virus particles released from an infected M2 cell [63, 80]	50 – 8000 (2000)	$\frac{\text{PFU}}{\text{cells}}$	0.2 – 32 (8)
ω	natural death rate of oncolytic viruses [16, 26]	0.1 – 10 (2)	day^{-1}	0.1 – 10 (2)
δ_v	elimination rate of viruses by the M1 cells (guessed value)	10^{-6} – 10^{-1} (5×10^{-5})	day^{-1}	10^{-6}–10^{-1} (5×10^{-5})
h_u	Half-saturation constant for the tumour cells that can trigger an M1→M2 re-polarisation (guessed value)	10^0 – 10^6 (10^5)	cells/vol	10^{-9} – 10^{-3} (10^{-4})
h_v	half-saturation constant for the viruses to trigger a M2 → M1 re-polarisation (guessed value)	10^0 – 10^6 (10^5)	PFU/vol	10^{-11} – 10^{-5} (10^{-6})
h_m	half-saturation constant for M2 macrophages involved in pro-tumour/anti-tumour immune responses (guessed value)	10^0 – 10^6 (10^5)	cells/vol	2.5×10^{-9}– 2.5×10^{-3} (2.5×10^{-4})

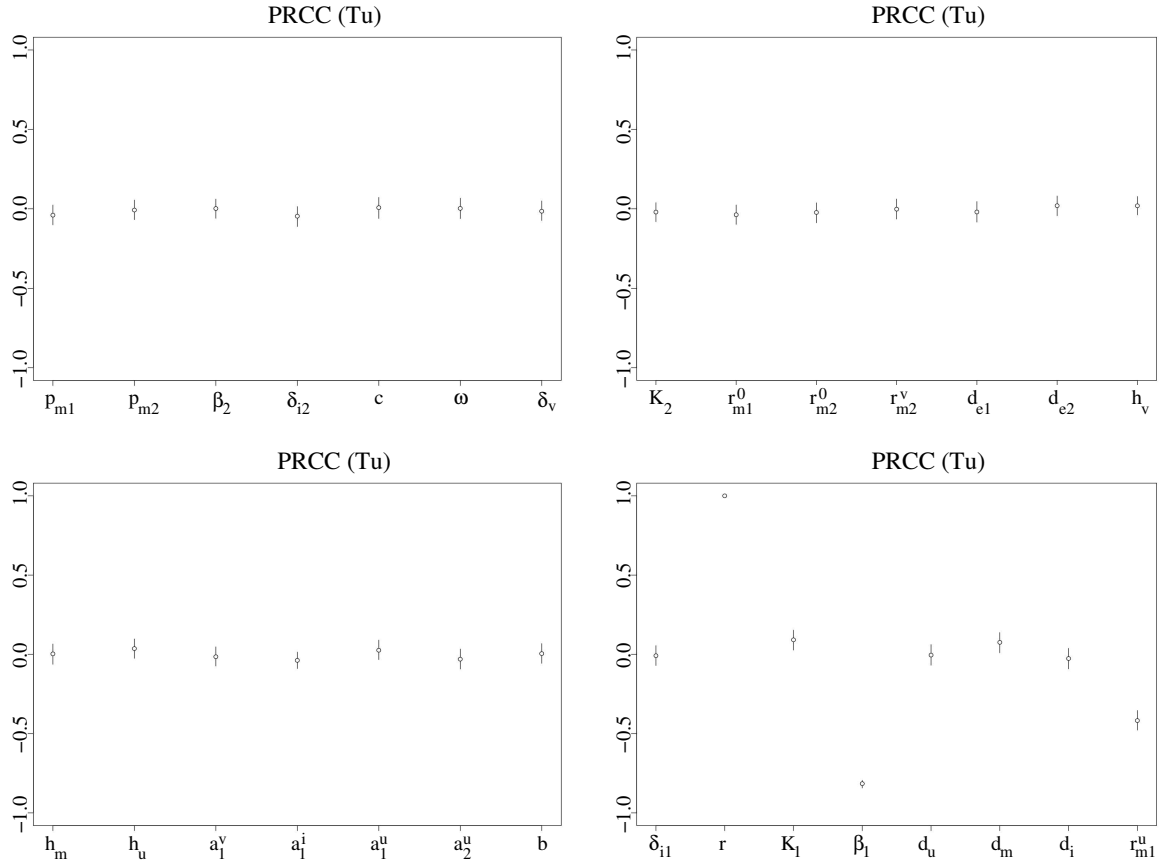

Figure 2. The effect of model parameters on T_u, as predicted by the LHS-PRCC analysis. Each parameter is sampled randomly 1000 times from the parameter ranges shown in Table 1, using a uniform distribution. We simulate tumour dynamics for 14 days (while the tumour exhibits a transient behaviour), with a time step of 1 day. The PRCC index varies between -1 and $+1$, and the largest PRCC index (in absolute value) corresponds to the parameter with respect to which the model outcome is most sensitive. We see that T_u is most sensitive to r, followed by β_1 and r^u_{m1}.

the numerical simulations in sections 3.2.1–3.2.2. The equilibria of (2.1a)–(2.1f) satisfy the following equations:

$$rT_u^*\left(1-\frac{T_u^*}{K_1}\right)-\beta_1 V^* T_u^* - d_u T_u^* \frac{M_1^*}{h_m + M_{2u}^*} + d_m T_u^* \frac{M_{2u}^*}{h_m + M_{2u}^*} = 0, \tag{3.1a}$$

$$\beta_1 V^* T_u^* - \delta_{i1} T_i^* - d_i T_i^* \frac{M_1^*}{h_m + M_{2u}^*} = 0, \tag{3.1b}$$

$$a_1^v V^* + a_1^i T_i^* + a_1^u T_u^* + p_{m1} M_1^* \left(1 - \frac{M_1^* + M_{2u}^*}{K_2}\right) - d_{e1} M_1^* -$$
$$M_1^* \left(r_{m1}^0 + r_{m1}^u \frac{T_u^*}{h_u + T_u^*}\right) + M_{2u}^* \left(r_{m2}^0 + r_{m2}^v \frac{V^*}{h_v + V^*}\right) = 0, \tag{3.1c}$$

$$a_2^u T_u^* + p_{m2} M_{2u}^* \left(1 - \frac{M_1^* + M_{2u}^*}{K_2}\right) + M_1^* \left(r_{m1}^0 + r_{m1}^u \frac{T_u^*}{h_u + T_u^*}\right) -$$

$$d_{e2} M_{2u}^* - M_{2u}^* \left(r_{m2}^0 + r_{m2}^v \frac{V^*}{h_v + V^*}\right) - \beta_2 V M_{2u}^* = 0, \tag{3.1d}$$

$$\beta_2 V^* M_{2u}^* - \delta_{i2} M_{2i}^* = 0, \tag{3.1e}$$

$$b\,\delta_{i1} T_i^* + c\,\delta_{i2} M_{2i}^* - \omega V^* - \delta_v V^* \frac{M_1^*}{h_m + M_{2u}^*} = 0. \tag{3.1f}$$

As mentioned in the previous section, since we do not have data which differentiates between the proliferation rates for M1 and M2 cells, we assume that $pm1 = pm2 := pm$ (see Table 1). Under these assumptions, model (2.1) exhibits two general types of equilibria: tumour-free steady states (summarised in Proposition 1) and tumour-present steady states (summarised in Proposition 2).

Proposition 1. *Model (2.1) can exhibit the following three types of tumour-free steady states:*

(i) Tumour-Free, Virus-Free, $M_1/M_{2u}/M_{2i}$ Macrophages-Free state (TIVF):
$(T_u^*, T_i^*, M_1^*, M_{2u}^*, M_{2i}^*, V^*) = (0, 0, 0, 0, 0, 0)$.

(ii) Tumour-Free, Virus-Free, M_1/M_{2u} Macrophages-Present state (TVF):
$(T_u^*, T_i^*, M_1^*, M_{2u}^*, M_{2i}^*, V^*) = (0, 0, M_1^*, M_{2u}^*, 0, 0)$, *with M_1^* and M_{2u}^* given implicitly by the following equation (which is plotted in Figure 3(a) for the baseline parameter values given in Table 1):*

$$p_m(M_{2u}^* - M_1^*)\left(1 - \frac{M_1^* + M_{2u}^*}{K_2}\right) = M_{2u}^*(2r_{m2}^0 + d_{e2}) - M_1^*(2r_{m1}^0 + d_{e1}) \tag{3.2}$$

(iii) Tumour-Free, Virus-Present, $M_1/M_{2u}/M_{2i}$-Present state (TF):
$(T_u^*, T_i^*, M_1^*, M_{2u}^*, M_{2i}^*, V^*) = (0, 0, M_1^*, M_{2u}^*, M_{2i}^*, V^*)$, *with M_1^*, M_{2u}^*, M_{2i}^*, and V^* given implicitly by the following equations (the last two being plotted in Figure 3(b) for the baseline parameter values given in Table 1):*

$$M_{2i}^* = \frac{\beta_2 V^* M_{2u}^*}{\delta_{i2}}, \tag{3.3a}$$

$$M_1^* = \frac{(h_m + M_{2u}^*)(c\,\beta_2 M_{2u}^* - \omega)}{\delta_v}, \tag{3.3b}$$

$$p_m(M_{2u}^* - M_1^*)\left(1 - \frac{M_1^* + M_{2u}^*}{K_2}\right) = M_{2u}^*\left(2r_{m2}^0 + 2r_{m2}^v \frac{V^*}{h_v + V^*} + d_{e2}\right) -$$

$$M_1^*(2r_{m1}^0 + d_{e1}) + a_1^v V^* + \beta_2 V^* M_{2u}^*. \tag{3.3c}$$

From Eq (3.3b) it is clear that this TF steady state exists only when $M_{2u}^* > \frac{\omega}{c\,\beta_2}$.

Proposition 2. *Model (2.1) can exhibit the following two types of tumour-present steady states:*

(i') Tumour-Present, Virus-Free, M_1/M_{2u} Macrophages-Present states (VF):

$$(T_u^*, T_i^*, M_1^*, M_{2u}^*, M_{2i}^*, V^*) = (T_u^*, 0, M_1^*, M_{2u}^*, 0, 0),$$

where T_u^*, M_1^* and M_{2u}^* are given implicitly by the following equations (also plotted in Figure 3(c), after Eq (3.4a) was substituted into (3.4b)):

$$T_u^* = K_1\left(1 + \frac{d_m M_{2u}^* - d_u M_1^*}{r(h_m + M_{2u}^*)}\right), \tag{3.4a}$$

$$(a_2^u - a_1^u)T_u^* + 2r_{m1}^u M_1^* \frac{T_u^*}{h_u + T_u^*} + p_m(M_{2u}^* - M_1^*)\left(1 - \frac{M_1^* + M_{2u}^*}{K_2}\right) = M_{2u}^*(2r_{m2}^0 + d_{e2}) - M_1^*(2r_{m1}^0 + d_{e1}). \tag{3.4b}$$

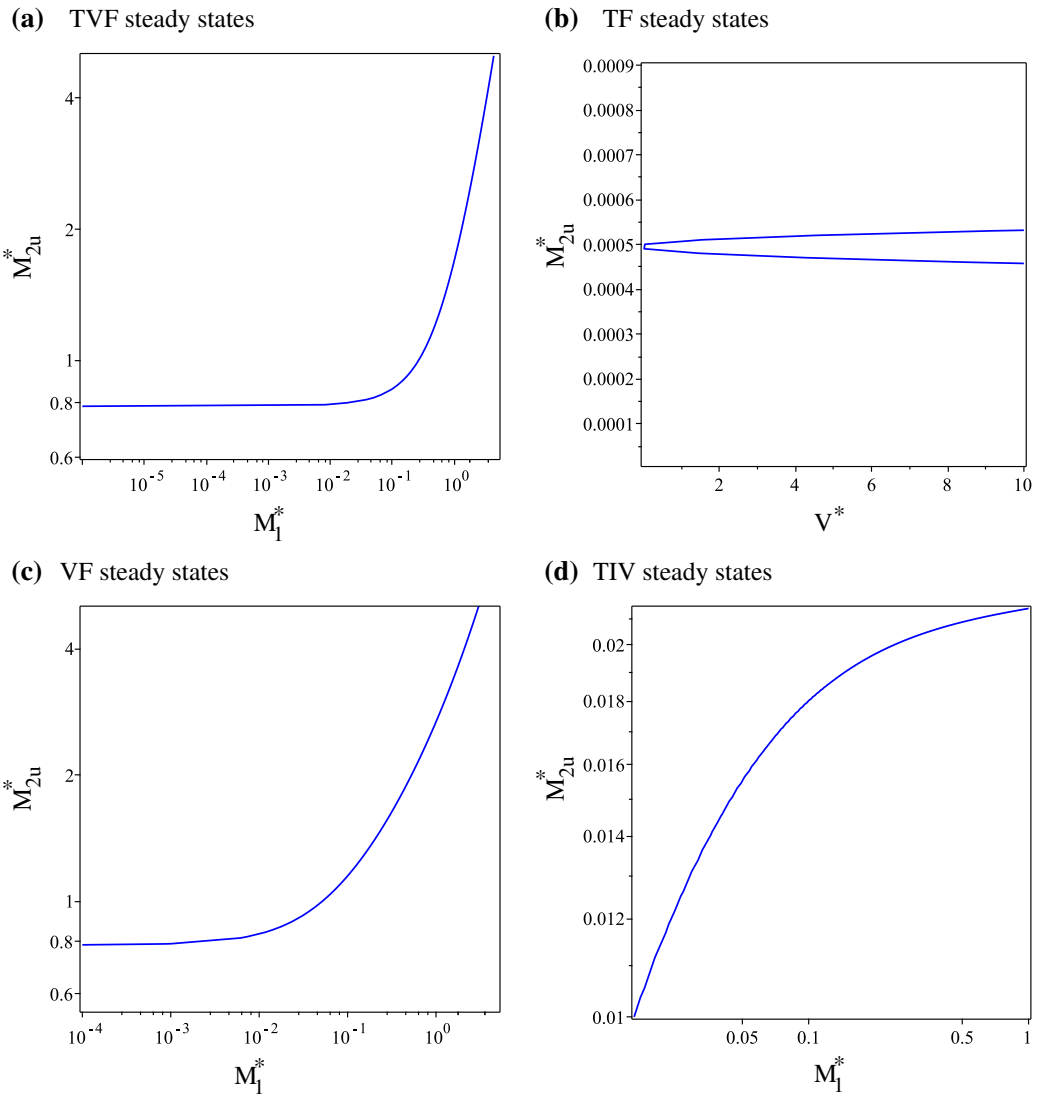

Figure 3. Summary of all non-zero steady states displayed by model (2.1), for the baseline parameters values shown in Table 1. (a) Plot of TVF steady states given by Eq (3.2), in the (M_1^*, M_{2u}^*) plane; (b) Plot of TF steady states given by Eqs (3.3b)–(3.3c), in the (V^*, M_{2u}^*) plane; (c) Plot of VF steady states given by Eq (3.4), in the (M_1^*, M_{2u}^*) plane; (d) Plot of TIV steady states given by Eqs (3.5a)–(3.5d), in the (M_1^*, M_{2u}^*) plane.

(ii') Tumour-Present, Virus-Present and $M_1/M_{2u}/M_{2i}$-Present states (TIV):

$$(T_u^*, T_i^*, M_1^*, M_{2u}^*, M_{2i}^*, V^*) = (T_u^*, T_i^*, M_1^*, M_{2u}^*, M_{2i}^*, V^*),$$

where the states are given implicitly by the following equations (also plotted in Figure 3(d) after substituting T_u^*, T_i^* and V^* in (3.5d)):

$$T_u^* = \frac{\delta_{i1} + d_i \frac{M_1^*}{h_m + M_{2u}^*}}{b\,\delta_{i1}\,\beta_1}\left(\omega + \frac{\delta_v M_1^*}{h_m + M_{2u}^*} - c\,\beta_2 M_{2u}^*\right), \tag{3.5a}$$

$$V^* = \frac{r}{K_1\,\beta_1}\left(K_1 + \frac{K_1}{r}\frac{(d_m M_{2u}^* - d_u M_1^*)}{(h_m + M_{2u}^*)} - T_u^*\right), \tag{3.5b}$$

$$T_i^* = \frac{\beta_1 V^* T_u^*}{\delta_{i1} + d_i \frac{M_1^*}{h_m + M_{2u}^*}}, \tag{3.5c}$$

$$\begin{aligned}&(a_2^u - a_1^u)T_u^* + 2r_{m1}^u M_1^* \frac{T_u^*}{h_u + T_u^*} + p_m(M_{2u}^* - M_1^*)\left(1 - \frac{M_1^* + M_{2u}^*}{K_2}\right) = \\ &M_{2u}^*(2r_{m2}^0 + d_{e2}) - M_1^*(2r_{m1}^0 + d_{e1}) + a_1^v V^* + a_1^i T_i^* + \beta_2 V^* M_{2u}^*.\end{aligned} \tag{3.5d}$$

In regard to Figure 3, where we plot the implicit expressions describing the various steady states, we note that for TVF, VF and TIV steady states, an increase in M1 cells is associated with an increase in the uninfected M2 cells. This is true also for the steady state TF (see Eq (3.3b)). Since the steady states TVF, TF, VF and TIV are too complex to calculate their closed-form expressions, in Figure 4 we show how they change as we vary two model parameters: (a) the tumour infection rate β_1, (b) the M2 macrophages infection rate β_2. We see that a decrease in β_1 below $\beta_1 = 729.9$ or an increase in β_2 above $\beta_2 = 5.9$ leads to the bifurcation of a TIV state (which contains tumour) from the TF state (with no tumour).

Stability of steady states. In the following we investigate analytically the stability of two of the steady states summarised in Proposition 1 – the simplest states, with no tumour and no virus. For the more complex steady states we will have to use numerical approaches to investigate their stability. We emphasise that this stability analysis will help us understand the numerical results presented in sections 3.2.1–3.2.2.

Proposition 3. *The tumour-free/virus-free/macrophages-free state (TIVF) and the tumour-free/virus-free/macrophage-present state (TVF) have the following stabilities:*

(i) The TIVF state is always unstable.

(ii) The TVF state is asymptotically stable provided that the following inequalities hold true:

$$M_1^* > \frac{rh_m + (d_m + r)M_{2u}^*}{d_u}, \tag{3.6a}$$

$$M_1^* + M_{2u}^* > \frac{K_2}{3p_m}[2p_m - (r_{m1}^0 + r_{m2}^0) - (d_{e1} + d_{e2})], \tag{3.6b}$$

$$\left[p_m\left(1 - \frac{M_1^* + M_{2u}^*}{K_2}\right) - d_{e1} - (r_{m1}^0 + r_{m2}^0)\right]\left[p_m\left(1 - 2\frac{M_1^* + M_{2u}^*}{K_2}\right) - d_{e2}\right] > 0. \tag{3.6c}$$

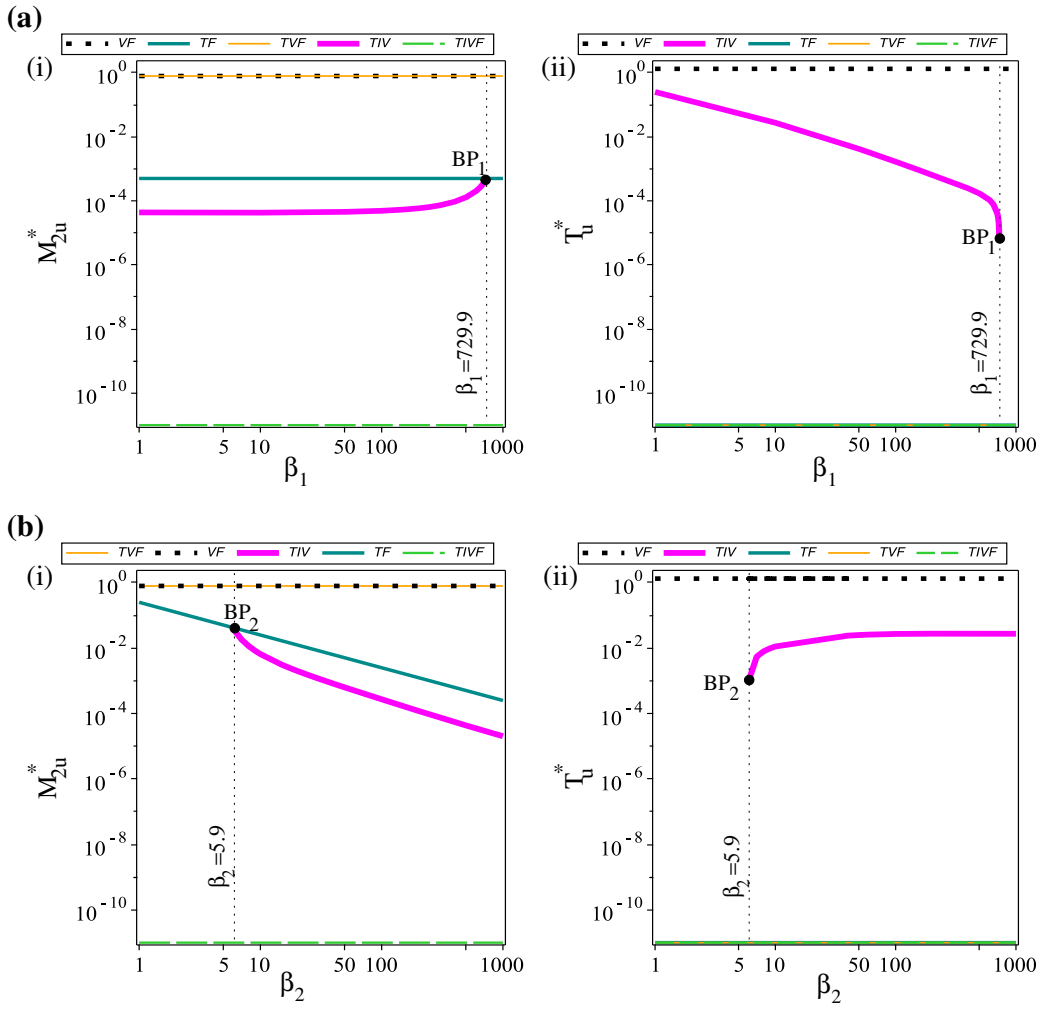

Figure 4. Bifurcation diagrams for all five steady states displayed by model (2.1) and summarised in Propositions 1–2, as we vary the infection parameters: (a) infection rate of tumour cells, $\beta_1 \in [1, 10^3]$; (b) infection rate of macrophages, $\beta_2 \in [1, 10^3]$. Sub-panels (i) show M_{2u}^* vs. parameter, while sub-panels (ii) show V^* vs parameter. All other parameter values that appear in model (2.1) are as in Table 1. Here "BP_1" denotes the bifurcation point where TIV steady state bifurcates out of the TF steady state as we decrease β_1 below $\beta_1 = 729.9$, and "BP_2" denotes the bifurcation point where TIV bifurcates out of TF as we increase β_2 above $\beta_2 = 5.9$.

Proof.

(i) The Jacobian matrix (see Eq (A.2) in Appendix C) associated with system (2.1) calculated at the TIVF steady state $(T_u^*, T_i^*, M_1^*, M_{2u}^*, M_{2i}^*, V^*) = (0, 0, 0, 0, 0, 0)$ *has always one positive eigenvalue* $\lambda_1 = r > 0$. *Thus this steady state is always unstable.*

(ii) The Jacobian matrix associated with system (2.1) calculated at the TVF steady state $(T_u^*, T_i^*, M_1^*, M_{2u}^*, M_{2i}^*, V^*) = (0, 0, M_1^*, M_{2u}^*, 0, 0)$ *has the following eigenvalues:*

$$\lambda_1 = r - \frac{d_u M_1^*}{h_m + M_{2u}^*} + \frac{d_m M_{2u}^*}{h_m + M_{2u}^*},$$

$$\lambda_2 = -\delta_{i1} - \frac{d_i M_1^*}{h_m + M_{2u}^*} < 0,$$
$$\lambda_3 = -\omega - \frac{\delta_v M_1^*}{h_m + M_{2u}^*} < 0,$$
$$\lambda_4 = -\delta i2 < 0,$$

and $\lambda_{5,6}$ *satisfying the quadratic equation*

$$\lambda^2 - \lambda(c_{11} + c_{22}) + c_{11}c_{22} - c_{12}c_{21} = 0,$$

with

$$c_{11} = p_m\left(1 - \frac{2M_1^* + M_{2u}^*}{K_2}\right) - r_{m1}^0 - d_{e1},$$
$$c_{12} = r_{m2}^0 - \frac{p_{m1}M_1^*}{K_2}, \quad c_{21} = r_{m1}^0 - \frac{p_{m2}M_{2u}^*}{K_2},$$
$$c_{22} = p_m\left(1 - \frac{M_1^* + 2M_{2u}^*}{K_2}\right) - r_{m2}^0 - d_{e2}.$$

This steady state is stable if $\lambda_1 < 0$ *and* $\lambda_{5,6} < 0$.

- *Condition* $\lambda_1 < 0$ *leads to the following inequality between the steady state values for M1 cells and uninfected M2 cells:*

$$M_1^* > \frac{r\, h_m + (d_m + r)M_{2u}^*}{d_u}.$$

- *Condition* $\lambda_{5,6} < 0$ *holds true if* $c_{11} + c_{22} < 0$ *and* $c_{11}c_{22} - c_{12}c_{21} > 0$. *When* $p_{m1} = p_{m2} := p_m$ *these last two inequalities are equivalent to*

$$p_m\left(2 - 3\frac{M_1^* + M_{2u}^*}{K_2}\right) - (d_{e1} + d_{e2}) < r_{m1}^0 + r_{m2}^0 \qquad \textit{and}$$
$$\left[p_m\left(1 - \frac{M_1^* + M_{2u}^*}{K_2}\right) - d_{e1} - (r_{m1}^0 + r_{m2}^0)\right]\left[p_m\left(1 - 2\frac{M_1^* + M_{2u}^*}{K_2}\right) - d_{e2}\right] > 0.$$

This completes the proof.

Remark 4. *Note that the stability of TF, VF, and TIV steady states is very difficult to investigate analytically, due to the complexity of the model and the fact that all these states are defined implicitly; see Eqs (3.3)–(3.5d). Even the stability conditions (3.6) for the TVF state are not straightforward to understand, since they depend on the implicit expression (3.2) connecting* M_1^* *and* M_2^*.

To address the analytical issues highlighted in the above Remark, in Figure 5 we investigate numerically the stability of steady states exhibited by model (2.1), as we vary the two infection parameters: $\beta_1, \beta_2 \in (1, 1000)$. Since the TIVF state is always unstable, we do not show it here. We note that TVF and VF steady states are always unstable when varying β_1 and β_2. An interesting dynamics is observed for the TF state when we vary β_2 (see panels (c)(ii), (d)(ii) and (e)). As β_2 increases towards $\beta_2^* = 10.5$ the larger amplitude limit cycle around the unstable TF point becomes unstable, and a smaller amplitude limit cycle emerges. This stable limit cycle evolves around the unstable TIV point.

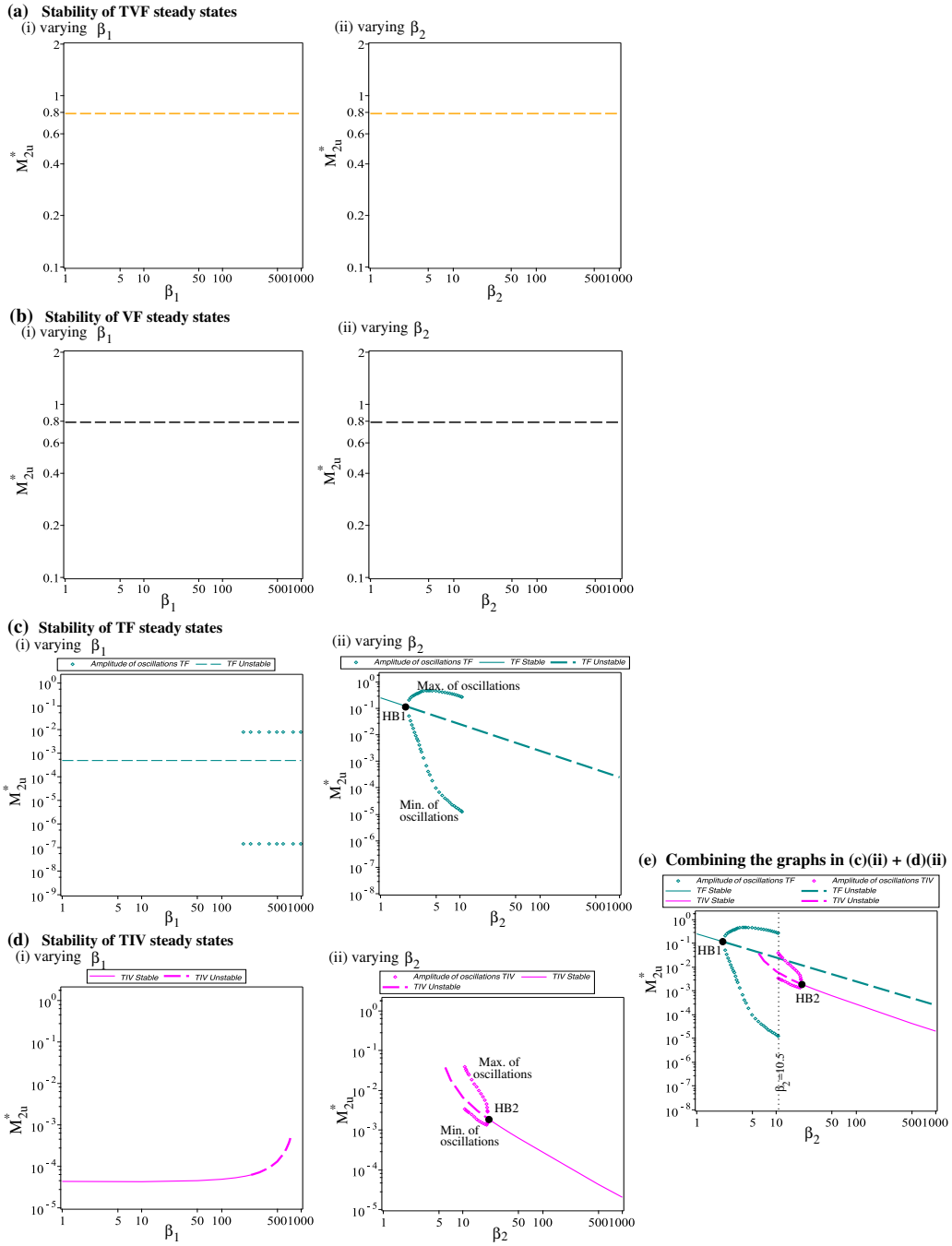

Figure 5. Stability of (a) TVF, (b) VF, (c) TF and (d) TIV steady states, as we vary the infection rates: (i) $\beta_1 \in [0, 1000]$ and (ii) $\beta_2 \in [0, 1000]$. Here we do not show the stability of TIVF since according to the Proposition 3 this steady state is always unstable (for all model parameters). Continuous curves show stable states and stable limit cycles, while dashed curves show unstable steady states (the unstable limit cycles were difficult to be traced, so we do not show them here). Dotted curves show the max/min of the stable oscillations when we have periodic solutions as a result of Hopf bifurcations. In sub-panel (e) we show on the same axes the graphs in (c)(ii) and (d)(ii), to emphasise the two Hopf bifurcation points "HB1" and "HB2", and the two limit cycles with different amplitudes that exchange stability at $\beta_2 = 10.5$. The rest of parameter values are presented in Table 1.

3.2. Numerical results

Numerical approach. To approximate numerically the ODE system (2.1), which might become stiff due to small and large parameter values (see Table 1), here we use an implicit 3rd order Rosenbrock method [65].

Initial conditions. The initial conditions for the time-evolution of model (2.1), summarised also in Table 2, were chosen to replicate some of the experimental conditions for tumour-macrophage-VSV dynamics from [25]. In [25], VSV was added to a plate with 5×10^5 MDA-MB231 human breast cancer cells, at a multiplicity of infection (MOI) of 1 or 10 PFU/cells. Here, we assume an average MOI of 2, and thus consider $V(0) = 10^6$PFU. The experiment in [25] considered the same number of macrophages and tumour cells (i.e., 5×10^5). Since in this study we investigate the activation/proliferation of M1 and M2 cells, as well as the M1→M2 polarisation (as tumour progresses) and M2→M1 re-polarisation (triggered by the VSV), here we start with much lower levels of M1 and M2 macrophages, and with more M1 than M2 cells; see also Table 2.

Table 2. Summary of initial conditions used for the numerical simulations of system (2.1).

Variable	Description	Initial conditions	Rescaled initial conditions
T_u	Density of uninfected tumour cells (cell numbers per volume)	$T_u(0) = 5 \times 10^5$	$T_u(0) = 5 \times 10^{-4}$
T_i	Density of infected tumour cells (cell numbers per volume)	$T_i(0) = 0$	$T_i(0) = 0$
M_1	Density of M1 macrophages (cell numbers per volume)	$M_1(0) = 10^3$	$M_1(0) = 2.5 \times 10^{-6}$
M_{2u}	Density of uninfected M2 macrophages (cell numbers per volume)	$M_{2u}(0) = 10^2$	$M_{2u}(0) = 2.5 \times 10^{-7}$
M_{2i}	Density of infected M2 macrophages (cell numbers per volume)	$M_{2i}(0) = 0$	$M_{2i}(0) = 0$
V	Density of virus particles (plaque-forming units (PFU) per volume)	$V(0) = 10^6$	$V(0) = 10^{-5}$

Remark 5. *We emphasise that there are very few experimental studies that investigate the interactions between the tumour cells, macrophages and oncolytic viruses – VSV in particular [25, 42, 43]. Most of the experimental studies existent in the literature record the dynamics of macrophages in general, without distinguishing the anti-viral/pro-viral roles of this heterogeneous population of cells [42, 43]. Among the very few experimental studies we found to distinguish the anti-tumour/pro-tumour and anti-viral/pro-viral roles of macrophages, we used [25] to generate the initial conditions for our mathematical model. Note that some of the experimental results in [25] (which did not include tumour explicitly, but focused on macrophages infection with VSV) were published very recently in [60].*
This scarcity of experimental results did not allow us to parametrise model (2.1) using one single experimental study, and thus many parameters were "guessed"; see section 2.1.

3.2.1. Baseline model dynamics

We start the investigation into the dynamics of model (2.1) by showing in Figure 6 the baseline dynamics obtained for the parameter values listed in Table 1. In sub-panel (a) we show the time

evolution of model variables, while in sub-panel (b) we graph the percentage of macrophages in the system (since various studies consider the percentage of macrophages as a predictor for tumour relapse [9]). We see that the increase in viral load leads to tumour elimination by day $t = 16$. The increase in M2 cells for $t \in (20, 30)$ leads to an un-detected growth in tumour population. This growth is faster and becomes detectable for $t > 50$, and is the result in a decrease in the M1 cell population around $t \approx 50$. The role of M1 and M2 macrophages in tumour relapse can be seen more clearly in sub-panel (b).

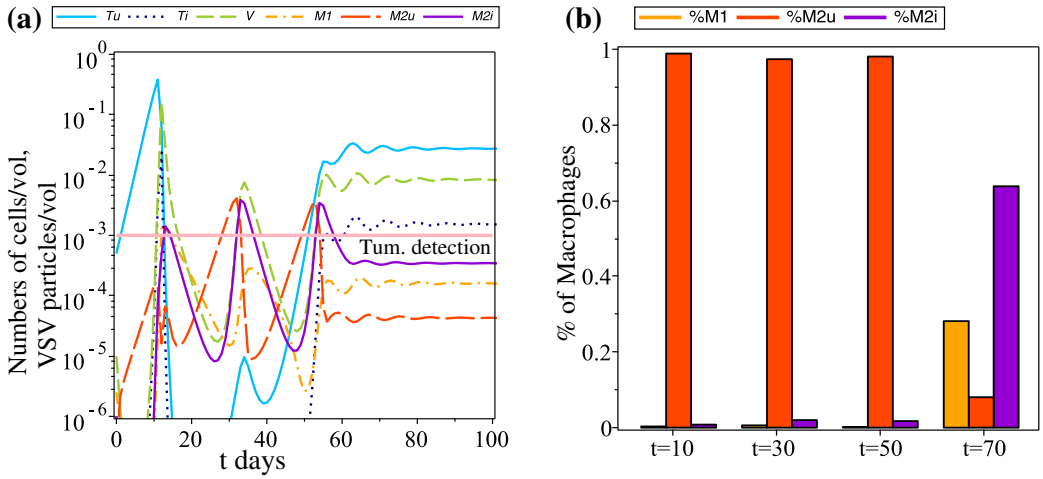

Figure 6. Dynamics of model (2.1) for the baseline parameter values listed in Table 1, with the initial conditions listed in Table 2. Sub-panel (a) shows virus-macrophages-tumour interactions. The thick horizontal pink line shows the detection level of the tumour (see Remark 3). Sub-panel (b) shows the percentages of M1 cells, as well as uninfected and infected M2 cells, at four specific days: $t = 10$, $t = 30$, $t = 50$ and $t = 70$.

3.2.2. Numerical results: transient and long-term behaviour as we vary model parameters

In the following we investigate numerically the dynamics of model (2.1) as we vary the rate of tumour cells infection with VSV (β_1) and the rate of M2 cells infection with VSV (β_2). We also investigate numerically the effect of varying the macrophages polarisation (r^u_{m1}) and re-polarisation (r^v_{m2}) rates (to address question (i) in the Introduction), and the effect of varying the viral bursts sizes c and b (to address question (ii) in the Introduction).

- In Figure 7(a),(b) we see that decreasing tumour infection rate $\beta_1 = 10 \to \beta_1 = 1$ (while fixing $\beta_2 = 500$) leads to a faster tumour relapse and a large tumour size. In Figure 7(c),(d) we see that decreasing the macrophage infection rate $\beta_2 = 10 \to \beta_2 = 1$ (while fixing $\beta_1 = 500$) leads to tumour elimination in the presence or absence of virus-immune oscillations.
- In Figure 8 we investigate the oscillatory dynamics observed above for small β_2. To this end, we fix $\beta_1 = \beta_2 = 1.4$ and vary the tumour-induced macrophages polarisation rate r^u_{m1}. We see that a decrease in this rate leads, in the long term, to a transition from regular oscillations (panels (a)) to chaotic oscillations (panels (c)). This chaotic dynamics occurs during tumour relapse; tumour seems to be eliminated before day $t = 35$, but relapse after day $t = 50$ in (b) and after day $t = 150$ in (c).

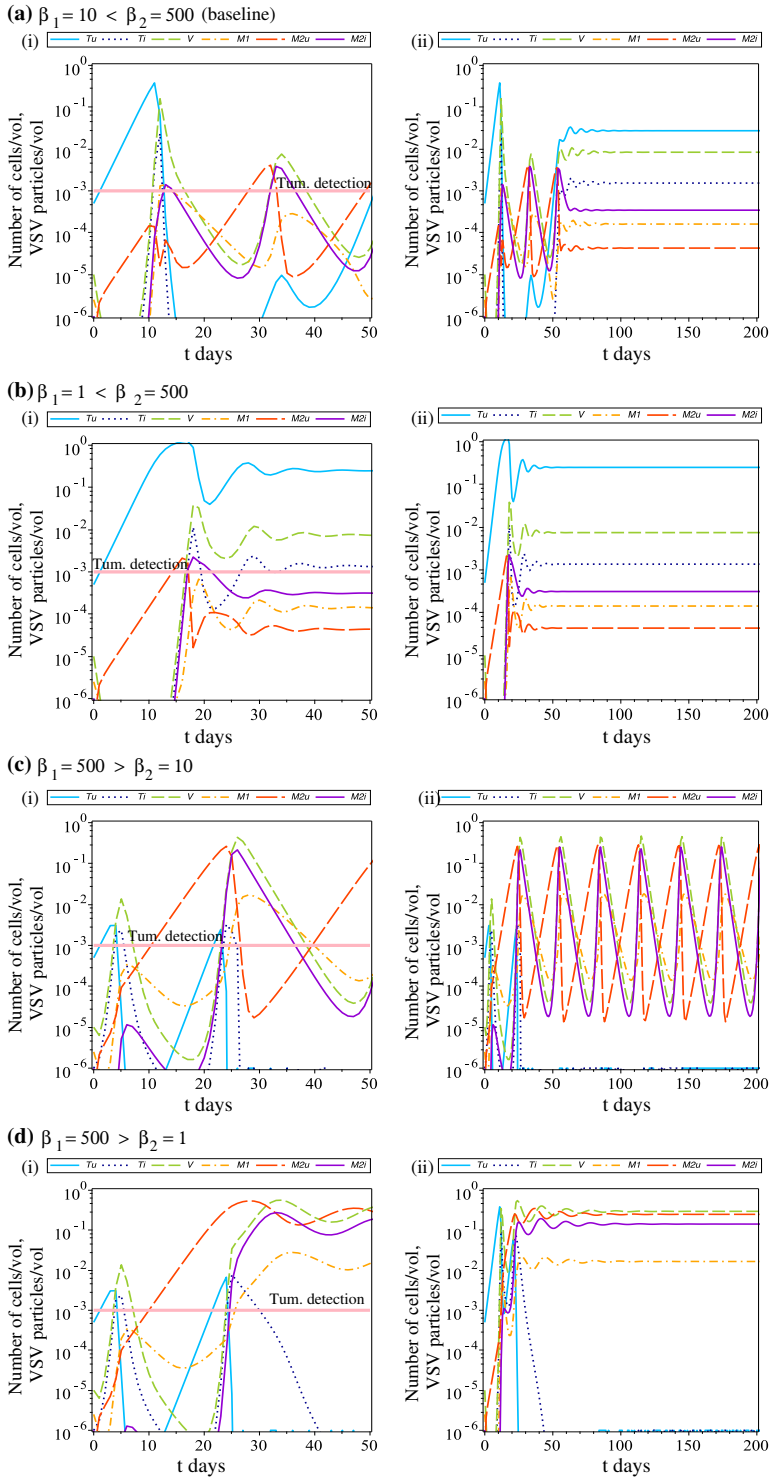

Figure 7. Dynamics of model (2.1) when we vary the infection rates. Sub-panels (i) show the short-term (transient) dynamics, while sub-panels (ii) show the long-term (asymptotic) dynamics. (a) $\beta_1 = 10 < \beta_2 = 500$; (b) $\beta_1 = 1 < \beta_2 = 500$; (c) $\beta_1 = 500 > \beta_2 = 10$; (d) $\beta_1 = 500 > \beta_2 = 1$.The rest of the parameters are as in the Table 1.

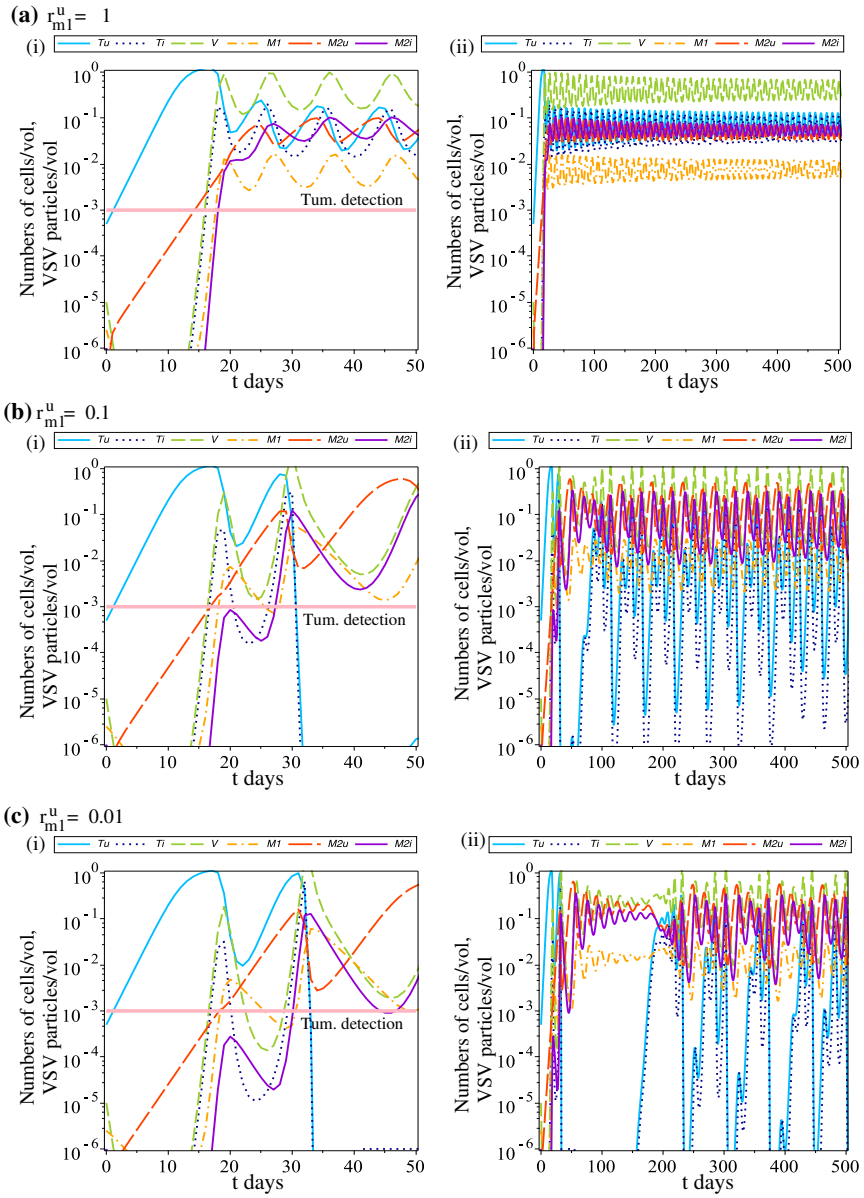

Figure 8. Dynamics of model (2.1), when we fix $\beta_1 = \beta_2 = 1.4$, and we vary r^u_{m1}. Sub-panels (i) show the short-term (transient) dynamics, while sub-panels (ii) show the long-term (asymptotic) dynamics. (a) $r^u_{m1} = 1$; (b) $r^u_{m1} = 0.1$; and (c) $r^u_{m1} = 0.01$. The rest of the parameters are as in the Table 1.

- In Figure 9 we investigate again the oscillatory dynamics observed above for small β_2, and how it changes as we vary the virus-induced macrophages re-polarisation rate r^v_{m2}. As we increase this rate, from $r^v_{m2} = 0.01$ in sub-panel (a) to $r^2_{m2} = 10$ in sub-panel (c) we see a loss in oscillations and a reduction/elimination of virus population. The virus particles are eliminated by the M1 cells, which cannot eliminate also the tumour cells.
- In Figure 10 we investigate the effect of varying the number of VSV particles released from infected M2 cells. We see that an increase in macrophages burst size from $c = 1$ (sub-panels (a)) to $c = 80$ (sub-panels (c)) leads to an increase in a transient immune-virus oscillatory dynamics,

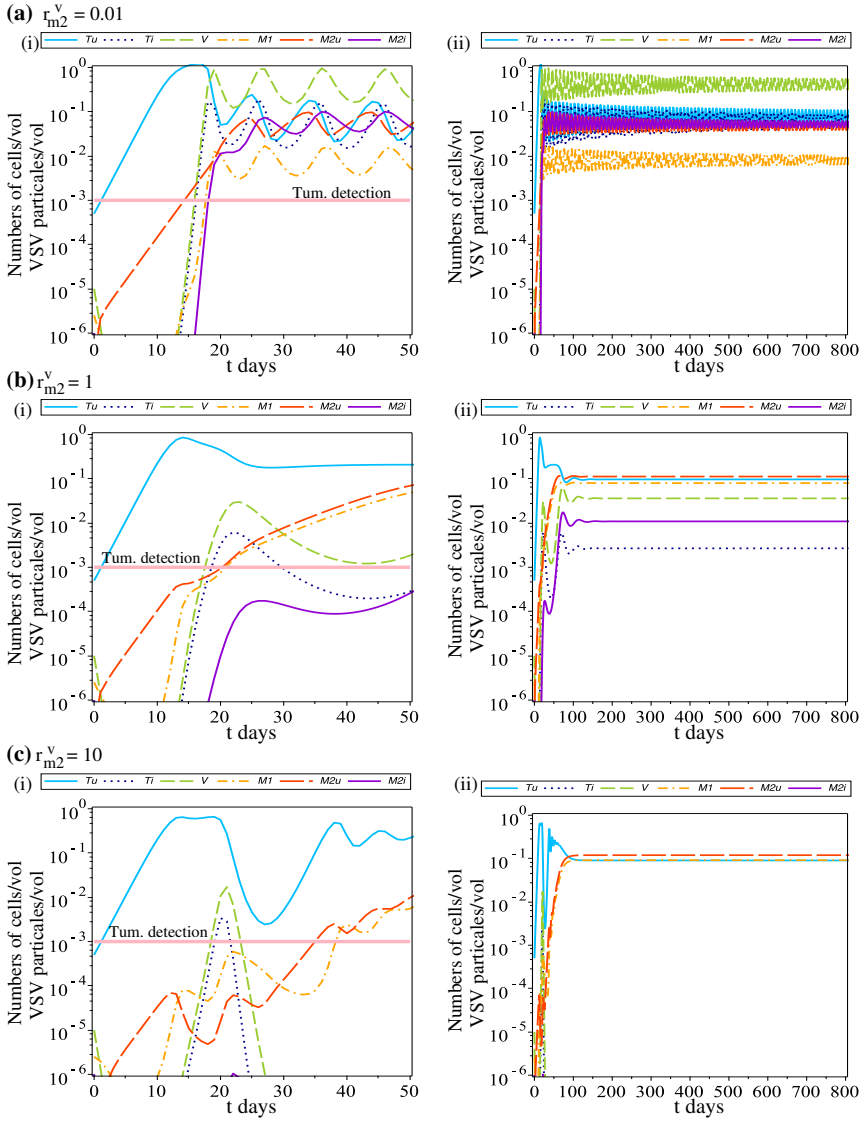

Figure 9. Dynamics of model (2.1), when we fix $\beta_1 = \beta_2 = 1.4$ and vary r^v_{m2}. Sub-panels (i) show the short-term (transient) dynamics, while sub-panels (ii) show the long-term (asymptotic) dynamics. (a) $r^v_{m2} = 0.01$, (b) $r^v_{m2} = 1$ and (c) $r^v_{m2} = 10$. The rest of the parameters are as in the Table 1.

which occurs when tumour is not detectable. In the long term, the tumour always approaches a steady state T^*_u, which increases with the ratio b/c (see panel (d)). For $b/c < 1$ this asymptotic tumour size decreases fast towards zero. For $b/c > 1$ this asymptotic tumour size increases at a much slower rate. These results suggest that the non-linearity in model dynamics plays a role in tumour evolution when the same number of virus particles are released by the infected tumour cells and infected macrophages. In particular, for the parameter values investigated here, larger macrophages burst sizes (c) have a bigger impact on tumour reduction compared to the tumour burst sizes (b).

The above results, on the effect of $\beta_1, \beta_2, r^u_{m1}, r^v_{m2}$ on tumour dynamics, are summarised in Table 3.

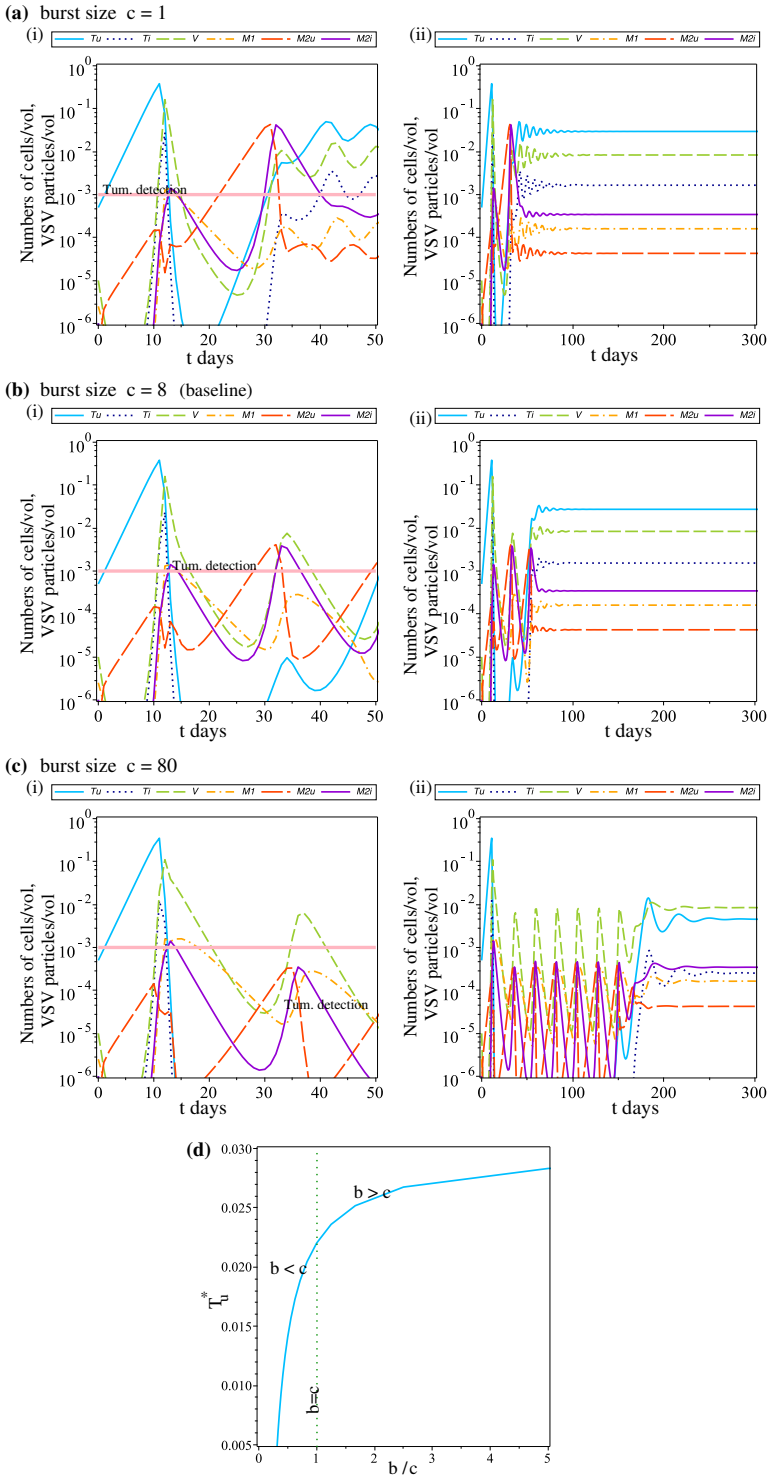

Figure 10. Dynamics model (2.1) when we vary c. Sub-panels (i) show the short-term (transient) dynamics, while sub-panels (ii) show the long-term (asymptotic) dynamics. (a) $c = 1$; (b) $c = 8$; (c) $c = 80$; (d) Changes in the steady-state tumour population T_u^* as we vary $c \in [5, 80]$ while we fix $b = 25$. The rest of the parameters are as in Table 1.

.

Table 3. Summary of the results shown in Figures 7–9.

Parameter	Results
$\beta_1 > \beta_2$	Tumour elimination, virus persistence.
$\beta_1 < \beta_2$	Tumour persistence, virus persistence.
$\beta_1 = \beta_2$, $(rm_1^u \downarrow)$	Chaotic dynamics.
$\beta_1 = \beta_2$, $(rm_2^v \uparrow)$	Steady states dynamics.

Periodic and chaotic oscillations. We have seen in Figure 8(c) that, for some specific parameter values, model (2.1) can exhibit chaotic dynamics. To have a better understanding of the short-term and long-term tumour behaviour corresponding to this case (where tumour seems to be eliminated periodically), in Figure 11 we graph the chaotic attractor corresponding to Figure 8(c), together with all the fixed points of model (2.1) (which will be discussed in more detail in section 3.1. We see that the tumour ($T_u^* + T_i^*$) is decreased towards zero due to the unstable tumour-present fixed points. The unstable tumour-free (TF) steady state resides in the chaotic attractor, while all other fixed points are outside the attractor. For comparison with the above chaotic attractor, in Figure 12 we show a periodic attractor. where the tumour is decreased to lower values but detectable values. The unstable tumour-free (TF) steady state resides in the middle of the periodic orbit, with the other fixed points (all unstable) being outside this orbit. Finally, we summarise these different asymptotic dynamics in Figure 13, where we show the regions in the (β_1, β_2) parameter space where we can find stable steady states (TF or TIV), stable limit cycles, and chaotic attractors.

4. Summary and discussions

In this paper, we considered a mathematical modelling and computational approach to investigate the complex interactions between tumour cells, an oncolytic virus – the Vesicular Stomatitis Virus (VSV) – and the innate immune response generated by the M1 and M2 macrophages, which can be found in large numbers inside different solid tumours. The novel aspect of this model is the possibility of infection of M2 cells with this oncolytic virus (as shown experimentally in [60]).

To understand the dynamics of this new (complex) mathematical model, we first focused on the steady states and their stability. Analytical results combined with numerical simulations were used to show how the steady states varied when we changed parameters related to cells' infection rates (i.e., β_1, β_2; see Figures 4 and 5). We mention here that a global sensitivity and uncertainty analysis using the classical LHS-PRCC approach identified β_1 as an parameter to which the uninfected tumour cells (T_u) are most sensitive to (see Figure 2); however, throughout this study we also wanted to compare the roles of β_1 and β_2 on the overall short-term and long-term tumour dynamics. Then, we used numerical simulations to investigate the transient and long-term dynamics of this model, as we varied the infection rates (β_1, β_2; see Figure 7), the tumour-induced M1→M2 polarisation rate (r_{m1}^u; see Figure 8), the virus-induced M2→M1 re-polarisation rate (r_{m2}^v; see Figure 9), and the viral burst size for tumour cells and macrophages (b, c; see Figure 10). Overall, numerical simulations showed a variety of asymptotic dynamics: from stable steady states, to stable limit cycles and chaotic oscillations (when all steady states were unstable). Given that for the parameter values used in this

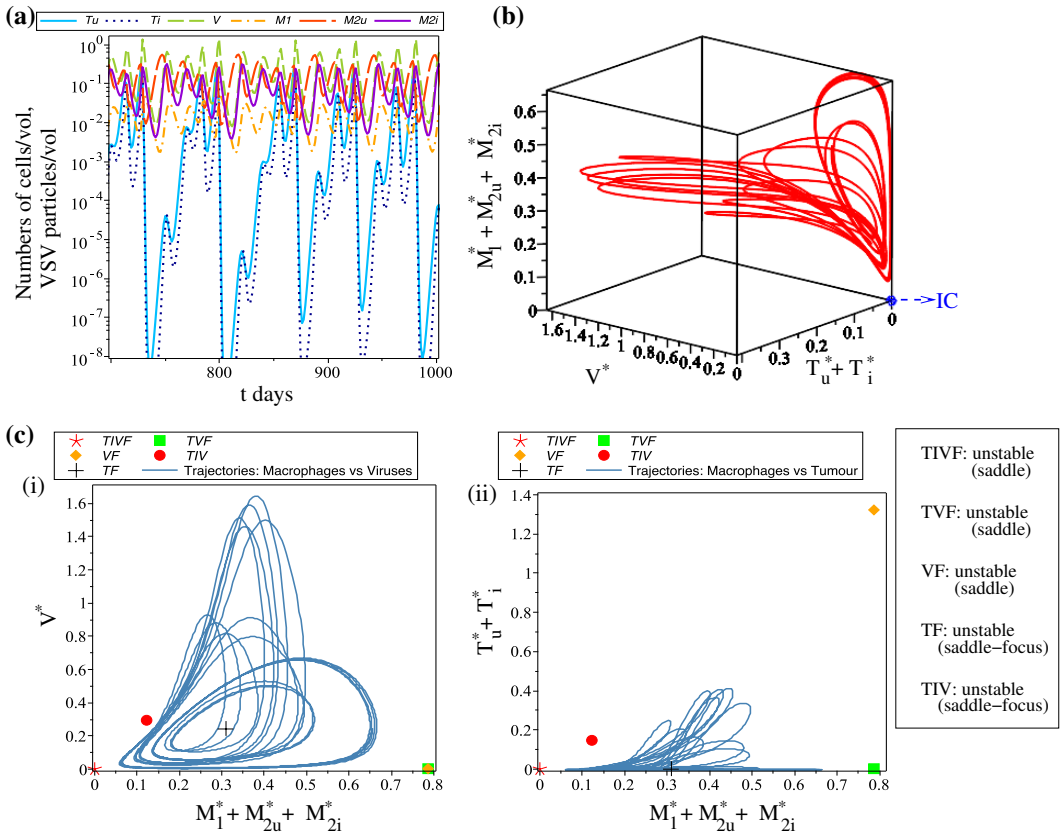

Figure 11. Chaotic attractor exhibited by model (2.1), when $r_{m1}^{u} = 0.01$ and $\beta_1 = \beta_2 = 1.4$ (all other parameters are as in Table 1): (a) Densities of cell/virus populations vs. time (for $t \in [700, 1000]$ days); (b) 3D phase plane plot showing macrophages vs. virus vs. tumour populations (for $t \in [700, 1000]$ days); (c) (i) Plot of solution trajectories in the (macrophage, virus) plane (for $t \in [700, 1000]$ days); (ii) Plot of solution trajectories in (macrophage, tumour) plane (for $t \in [700, 1000]$ days). In addition, we show the fixed points TIVF, TVF, VF, TF and TIV, corresponding to these parameter values.

study (many of which were guessed, due to a lack of experimental studies on both tumour and macrophage infections with oncolytic VSV) the regular and irregular oscillations were observed also above the tumour detection level (see Remark 3). To our knowledge, this is not a biologically realistic behaviour for aggressive breast cancers, as the majority of experimental *in vitro* and *in vivo* studies on the highly aggressive MDA-MB-231 cell line show exponential cancer growth [10, 71, 76], in the absence of any external treatment that could be periodically administered (and thus force a periodic decay/re-growth of tumour). Nevertheless, the results are interesting from a dynamical systems point of view, since they allow us to understand the whole range of possible dynamics exhibited by model (2.1).

Returning to the biological questions we raised at the end of the Introduction section, our computational results have suggested the following biological hypotheses:

(i) The increase in the macrophage tumour-induced polarisation rate r_{m1}^{u} leads to a fast tumour relapse (see Figure 8): from relapse on day $t \approx 170$ for $r_{m1}^{u} = 0.01$ to a relapse on day $t \approx 70$ for $r_{m1}^{u} = 0.1$

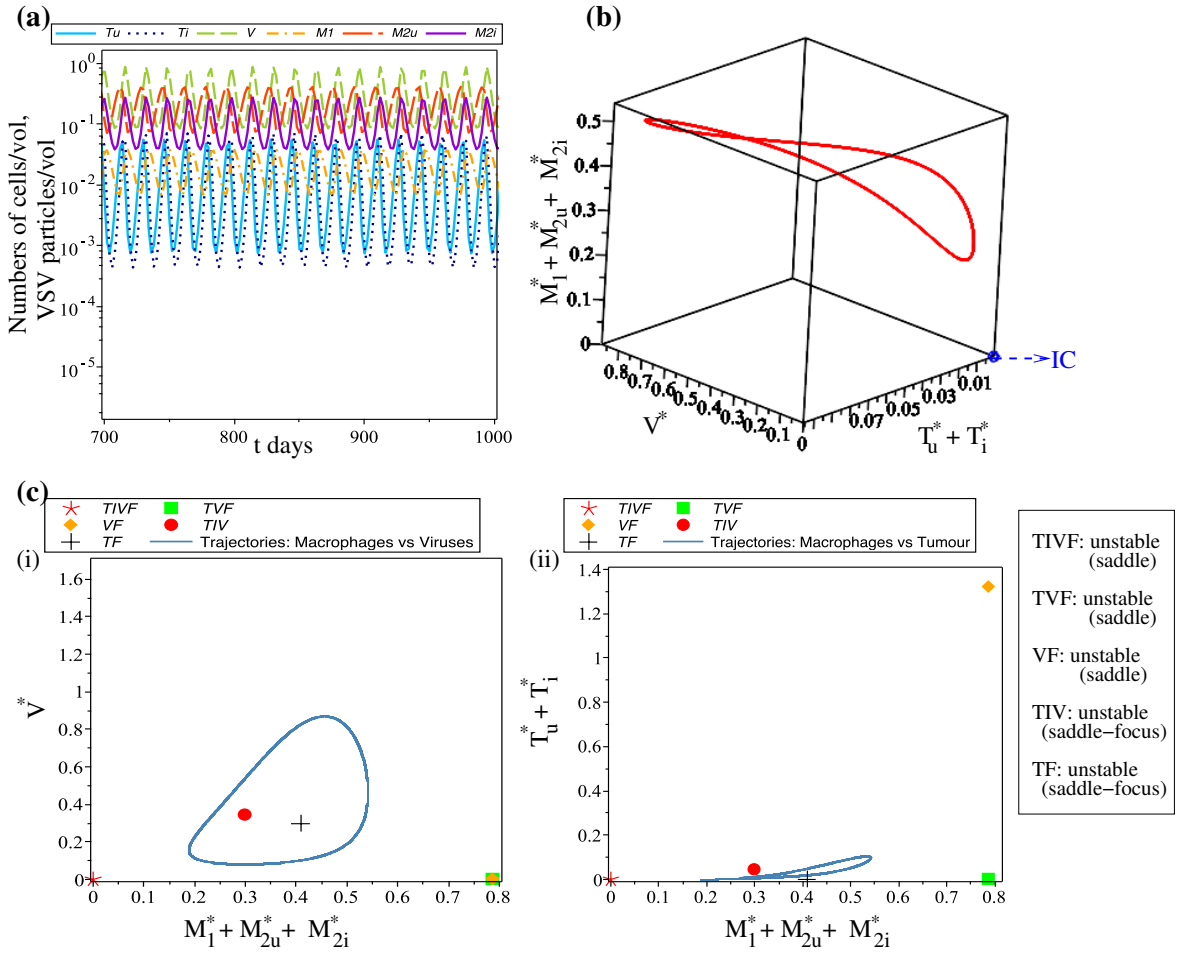

Figure 12. Periodic attractor exhibited by model (2.1), when $r^{u}_{m1} = 0.01$ and $\beta_1 = 2 > \beta_2 = 1$ (and all other parameters as in Table 1): (a) Densities of cell/virus populations vs. time (for $t \in [700, 1000]$ days); (b) 3D phase plane plot showing macrophages vs. virus vs. tumour populations (for $t \in [700, 1000]$ days); (c) (i) Phase plane for macrophages-virus plane, (ii) Phase plane for macrophages-tumour plane, (for $t \in [700, 1000]$). In addition, we show the fixed points TIVF, TVF, VF, TF and TIV (corresponding to these parameter values.)

.

and continuous tumour presence when $r^{u}_{m1} = 1.0$. The increase in the macrophage virus-induced re-polarisation rate r^{v}_{m2} can lead to a tumour reduction (but not elimination) for as long as the virus is present in the system (see Figure 9).

(ii) Changes in the infection rate of macrophages, β_2 (for large β_1, which lead to tumour elimination) seems to lead to a transition between a state characterised by oscillations in immune response to a state characterised by an immune-only steady state (see Figure 7 (c),(d)). We do not know yet if such oscillations in immune response (which take place over multiple days) are realistic from a biological point of view.

The increase in the infection rate of tumour cells, β_1 (for large β_2) leads to a delay in tumour relapse (see Figure 7(a),(b)).

(iii) In regard to VSV replication inside macrophages vs. tumour cells, and the release of these

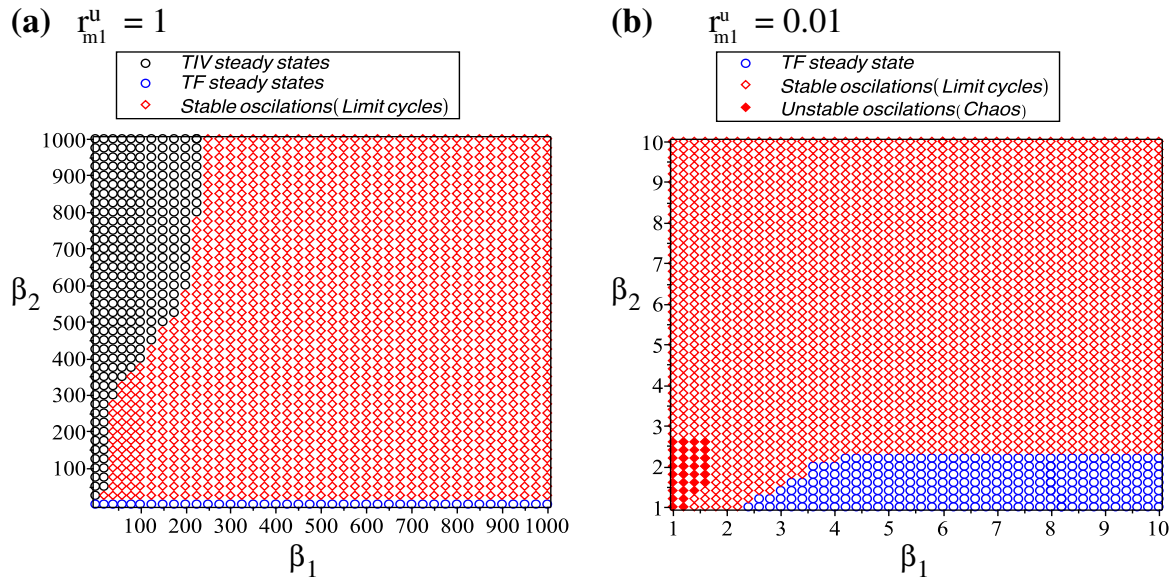

Figure 13. Summary of asymptotic dynamics in the (β_1, β_2) plane. (a) $r^u_{m1} = 1$, and $\beta_{1,2} \in (1, 1000)$. (b) $r^u_{m1} = 0.01$, and $\beta_{1,2} \in (1, 10)$.

particles from the lysed cells, we note that $b > c$ is associated with a fast tumour relapse after a temporary reduction in tumour size. In contrast, $c > b$ is associated with an increase in tumour relapse. Moreover, the tumour seems to be more sensitive changes in macrophages burst size c compared to tumour burst size b (see Figure 10).

Since the VSV-infected macrophages do not release immediately the virus particles, being able to act as reservoirs of VSV gRNA [54,68], our current work in progress focuses on the impact of delayed release of VSV particles from the infected macrophages. Also, since infected M2 macrophages can deliver oncolytic viruses to hypoxic areas of the tumour [53] another current research direction focuses on the migration of macrophages that can be infected with VSV, and their interactions with the tumour cells.

To conclude this discussion, we emphasise that the mathematical models derived to investigate specific aspects of tumour-immune interactions and different immunotherapies for cancer are becoming more and more complex, thus acknowledging the complex biological interactions that made it impossible until now to find a cure for cancer. But this increased model complexity also forces us to rely more and more heavily on computational approaches to understand model dynamics, and to make biologically-testable predictions.

Acknowledgments

The authors received no financial support for the research, authorship, and/or publication of this article.

Conflict of interest

The authors declare no conflict of interest.

References

1. M. Ahmed, S. Cramer, D. Lyles, Sensitivity of prostate tumours to wild type and m protein mutant vesicular stomatitis viruses, *Virology*, **330** (2004), 34–49.
2. P. Allavena, A. Mantovani, Immunology in the clinic review series; focus on cancer: tumour-associated macrophages: undisputed stars of the inflammatory tumour microenvironment, *Clin. Exp. Immunol.*, **167** (2012), 195–205.
3. P. Allavena, A. Sica, C. Garlanda, A. Mantovani, The yin-yang of tumour-associated macrophages in neoplastic progression and immune surveillance, *Immunol. Rev.*, **222** (2008), 155–161.
4. N. Almuallem, R. Eftimie, A mathematical model for the role of macrophages in the persistence and elimination of oncolytic viruses, *Math. Appl. Sci. Eng.*, **1** (2020), 126–149.
5. S. Blower, H. Dowlatabadi, Sensitivity and uncertainty analysis of complex models of disease transmission: an HIV model, as an example, *Int. Stat. Rev.*, **62** (1994), 229–243.
6. M. Boemo, H. Byrne, Mathematical modelling of hypoxia-regulated oncolytic virus delivered by tumour-associated macrophages, *J. Theor. Biol.*, **461** (2019), 102–116.
7. B. Bridle, J. Boudreau, B. Lichty, J. Brunelliére, K. Stephenson, S. Koshy, et al., Vesicular stomatitis virus as a novel cancer vaccine vector to prime antitumour immunity amenable to rapid boosting with adenovirus, *Mol. Ther.*, **17** (2009), 1814–1821.
8. M. J. Brown, S. Bahsoun, M. Morris, E. Akam, Determining conditions for successful culture of multi-cellular 3D tumour spheroids to investigate the effect of mesenchymal stem cells on breast cancer cell invasiveness, *Bioengineering*, **6** (2019), 101.
9. X. Y. Chen, A. Thike, N. Nasir, V. Koh, B. Bay, P. Tan, Higher density of stromal M2 macrophages in breast ductal carcinoma in situ predicts recurrence, *Virchows Archiv.*, **476** (2020), 825–833.
10. R. Y. S. Cheng, N. L. Patel, T. Back, D. Basudhar, V. Somasundaram, J. D. Kalen, et al., Studying triple negative breast cancer using orthotopic breast cancer model, *J. Vis. Exp.*, **157** (2020), e60316.
11. V. Chitu, Y. G. Yeung, W. Yu, S. Nandi, E. R. Stanley, Measurement of macrophage growth and differentiation, *Curr. Protoc. Immunol.*, **92**, (2011), 14–20.
12. M. Cobleigh, C. Bradfield, Y. Liu, A. Mehta, M. Robek, The immune response to a Vesicular Stomatitis Virus vaccine vector is independent of particulate antigen secretion and protein turnover rate, *J. Virology*, **86**, (2012), 4253–4261.
13. E. Corbin, O. Adeniba, O. Cangellaris, W. King, R. Bashir, Evidence of differential mass change rates betwen human breast cancer cell lines in culture, *Biomed. Microdevices*, **19**, (2017), 10.
14. N. De Silva, H. Atkins, D. H. Kirn, J. C. Bell, C. J. Breitbach, Double trouble for tumours: exploiting the tumour microenvironment to enhance anticancer effect of oncolytic viruses, *Cytokine Growth Factor Rev.*, **21**, (2010), 135–141.
15. N. Denton, C. Y. Chen, T. Scott, T. Cripe, Tumour-associated macrophages in oncolytic virotherapy: friend or foe? *Biomedicines*, **4** (2016), 13.
16. N. DePolo, J. Holland, The intracellular half-lives of nonreplicating nucleocapsids of DI particles of wild type and mutant strains of vesicular stomatitis virus, *Virology*, **151** (1986), 371–378.

17. R. Eftimie, J. Dushoff, B. W. Bridle, J. L. Bramson, D. J. Earn, Multi-stability and multi-instability phenomena in a mathematical model of tumor-immune-virus interactions, *Bull. Math. Biol.*, **73** (2011), 2932–2961.

18. R. Eftimie, G. Eftimie, Tumour-associated macrophages and oncolytic virotherapies: a mathematical investigation into a complex dynamics, *Lett. Biomath.*, **5** (2018), S6–S35.

19. R. Eftimie, G. Eftimie, Investigating macrophages plasticity following tumour–immune interactions during oncolytic therapies, *Acta Biotheor.*, **67** (2019), 321–359.

20. R. Eftimie, H. Hamam, Modelling and investigation of the CD4+ T cells–macrophages paradox in melanoma immunotherapies, *J. Theor. Biol.*, **420** (2017), 82–104.

21. R. Eftimie, C. K. Macnamara, J. Dushoff, J. L. Bramson, D. J. Earn, Bifurcations and chaotic dynamics in a tumour-immune-virus system. *Math. Model. Nat. Phenom.*, **11** (2016), 65–85.

22. R. van Furth, I. Elzenga-Claasen, M. van Schdewijk-Nieuwstad, M. M. Diesselhoff-den, H. Toivonen, T. Rytömaa, Cell kinetic analysis of a murine macrophage cell line, *Eur. J. Cell Biol.*, **44** (1987), 93–96.

23. J. Fournier, O. Robain, I. Cerutti, I. Tardivel, F. Chany-Fournier, C. Chany, Detection of vesicular stomatitis virus (VSV) RNA in the central nervous system of infected mice by in situ hybridization, *Acta Neuropathol.*, **75** (1988), 554–556.

24. S. Friberg, S. Mattson, On the growth rates of human malignant tumours: implications for medical decision making, *J. Surg. Oncol.*, **65** (1997), 284–297.

25. R. Fuller, *Response of M2 Macrophages in a Simulated Tumor Microenvironment to Infection with Vesicular Stomatitis Virus*, Master's thesis, Appalachian State University, 2018.

26. Y. Gao, P. Whitaker-Dowling, S. Watkins, J. Griffin, I. Bergman, Rapid adaptation of a recombinant vesicular stomatitis virus to a targeted cell line, *J. Virol.*, **80** (2006), 8603–8612.

27. D. Gong, W. Shi, S. Yi, H. Chen, J. Groffen, N. Heisterkamp, TGFβ signalling plays a critical role in promoting alternative macrophage activation, *BMC Immunol.*, **13** (2012), 31.

28. C. Guiducci, A. P. Vicari, S. Sangaletti, G. Trinchieri, M. P. Colombo, Redirecting in vivo elicited tumour infiltrating macrophages and dendritic cells towards tumour rejection, *Cancer Res.*, **65** (2005), 3437–3446.

29. C. Guiot, P. G. Degiorgis, P. P. Delsanto, P. Gabriele, T. S. Deisboeck, Does tumor growth follow a "universal law"? *J. Theor. Biol.*, **225** (2003), 147–151.

30. M. Hollmén, F. Roudnicky, S. Karaman, M. Detmar, Characterization of macrophage-cancer cell crosstalk in estrogen positive and triple-negative breast cancer, *Sci. Rep.*, **5** (2015), 9188.

31. P. Italiani, D. Boraschi, From monocytes to m1/m2 macrophages: phenotypical vs. functional differentiation, *Front. Immunol.*, **5** (2014), 514.

32. A. Jenner, P. Kim, F. Frascoli, Oncolytic virotherapy for tumours following a Gompertz growth law, *J. Theor. Biol.*, **480** (2019), 129–140.

33. A. Jenner, C. O. Yun, A. Yoon, A. Coster, P. Kim, Modelling combined virotherapy and immunotherapy, *Lett. Biomath.*, **5** (2018), S99–S116.

34. H. L. Kaufman, F. J. Kohlhapp, A. Zloza, Oncolytic viruses: a new class of immunotherapy drugs, *Nat. Rev. Drug Discovery*, **14** (2015), 642–662.
35. K. S. Kim, S. Kim, I. H. Jung, Hopf bifurcation analysis and optimal control of treatment in a delayed oncolytic virus dynamics, *Math. Comput. Simul.*, **149** (2018), 1–16.
36. P. Kim, J. Crivelli, I. K. Choi, C. O. Yun, J. Wares, Quantitative impact of immunomodulation versus oncolysis with cytokine-expressing virus therapeutics, *Math. Biosci. Eng.*, **12** (2015), 841–858.
37. A. Klepper, A. Branch, Macrophages and the viral dissemination super highway, *EC Microbiol.*, **2** (2015), 328–336.
38. A. Labonte, A. C. Tosello-Trampont, Y. Hahn, The role of macrophage polarisation in infectious and inflammatory diseases, *Mol. Cells*, **37** (2014), 275–285.
39. A. K. Laird, Dynamics of tumour growth: comparison of growth rates and extrapolation of growth curve to one cell, *Br. J. Cancer*, **19** (1965), 278.
40. P. Lang, M. Recher, N. Honke, S. Scheu, S. Borkens, N. Gailus, et al., Tissue macrophages suppress viral replication and prevent severe immunopathology in an Interferon-I-dependent manner in mice, *Hepatology*, **52** (2010), 25–32.
41. T. Lee, A. Jenner, P. S. Kim, J. Lee, Application of control theory in a delayed-infection and immune-evading oncolytic virotherapy, *Math. Biosci. Eng.*, **17** (2020), 2361–2383.
42. S. Leveille, M. L. Goulet, B. D. Lichty, J. Hiscott, Vesicular stomatitis virus oncolytic treatment interferes with tumour-associated dendritic cell functions and abrogates tumour antigen presentation, *J. Virol.*, **85** (2011), 12160–12169.
43. Y. P. Liu, L. Suksanpaisan, M. B. Steele, S. J. Russell, K. W. Peng, Induction of antiviral genes by the tumour microenvironment confers resistance to virotherapy, *Sci. Rep.*, **3** (2013), 2375.
44. X. Lu, R. Yang, L. Zhang, Y. Xi, J. Zhao, F. Wang, et al., Macrophage colony-stimulating factor mediates the recruitment of macrophages in triple negative breast cancer, *Int. J. Biol. Sci.*, **15** (2019), 2859–2871.
45. E. G. Lucero, *The Cytotoxic Effects of Vesicular Stomatitis Virus on the THP-1 Macrophages*, PhD thesis, Appalachian State University, 2018.
46. C. Macnamara, R. Eftimie, Memory versus effector immune responses in oncolytic virotherapies, *J. Theor. Biol.*, **377** (2015), 1–9.
47. G. Magombedze, S. Eda, V. V. Ganusov, Competition for antigen between Th1 and Th2 responses determines the timing of the immune response switch during mycobaterium avium subspecies paratuberulosis infection in ruminants, *PLoS Comput. Biol.*, **10** (2014), e1003414.
48. J. Malinzi, R. Ouifki, A. Eladdadi, D. F. Torres, K. White, Enhancement of chemotherapy using oncolytic virotherapy: mathematical and optimal control analysis, *Math. Biosci. Eng.*, **15** (2018), 1435–1463.
49. A. Mantovani, A. Sica, S. Sozzani, P. Allavena, A. Vecchi, M. Locati, The chemokine system in diverse forms of macrophage activation and polarisation, *Trends Immunol.*, **25** (2004), 677–686.
50. G. Marelli, A. Howells, N. R. Lemoine, Y. Wang, Oncolytic viral therapy and the immune system: a double-edged sword against cancer, *Front. Immunol.*, **9** (2018), 866.

51. S. Marino, I. Hogue, C. Ray, D. Kirschner, A methodology for performing global uncertainty and sensitivity analysis in systems biology, *J. Theor. Biol.*, **254** (2008), 178–196.
52. S. Morgensen, Macrophages and natural resistance to virus infections, in *Infection* (eds. M.R. Escobar and J.P. Utz), Springer, Boston, MA, (1988), 207–223.
53. M. Muthana, A. Giannoudis, S. Scott, H. Y. Fang, S. Coffelt, F. Morrow, et al., Use of macrophages to target therapeutic adenovirus to human prostate tumours, *Cancer Res.*, **71** (2011), 1805–1815.
54. E. Nikitina, I. Larionova, E. Choinzonov, J. Kzhyshkowska, Monocytes and macrophages as viral targets and reservoirs, *Int. J. Mol. Sci.*, **19** (2018), 2821.
55. A. Nikonova, M. Khaitov, D. Jackson, S. Taub, M. B. Tujillo-Torralbo, D. Kudlay, M1-like macrophages are potent producers of anti-viral interferons and M1-associated marker-positive lung macrophages are decreased during rhinovirus-induced asthma exacerbations, *EBioMedicine*, **54** (2020), 102734.
56. M. Nowak, R. M. May, *Virus Dynamics: Mathematical Principles of Immunology and Virology: Mathematical Principles of Immunology and Virology*, Oxford University Press, UK, 2000.
57. M. A. Nowak, C. R. Bangham, Population dynamics of immune responses to persistent viruses, *Science*, **272** (1996), 74–79.
58. S. Owen, *The type I interferon anti-viral pathway contributes to macrophage polarisation following infection with oncolytic vesicular stomatitis virus*, Master's thesis, Appalachian State University, 2020.
59. A. S. Perelson, Modelling viral and immune system dynamics. *Nat. Rev. Immunol.*, **2** (2002), 28.
60. M. Polzin, J. McCanless, S. Owen, D. Sizemore, E., R. Lucero, H. N. Fuller, et al., Oncolytic vesicular stomatitis viruses selectively target M2 macrophages, *Virus Res.*, **284** (2020), 197991.
61. M. A. Polzin, *Therapeutic targeting of macrophage populations by oncolytic vesicular stomatitis virus*, Master's thesis, Appalachian State University, 2017.
62. M. Ponzoni, F. Pastorino, D. Di Paolo, P. Perri, C. Brignole, Targeting macrophages as a potential therapeutic intervention: impact on inflammatory diseases and cancer, *Int. J. Mol. Sci.*, **19** (2018), 1953.
63. B. Rager-Zisman, M. Kunkel, Y. Tanaka, B. R. Bloom, Role of macrophage oxidative metabolism in resistance to vesicular stomatitis virus infection, *Infect. Immun.*, **36** (1982), 1229–1237.
64. A. Risinger, N. Dybdal-Hargreaves, S. Mooberry, Breast cancer cell lines exhibit differential sensitivities to microtubule-targeting drugs independent of doubling time, *Anticancer Res.*, **35** (2015), 5845–5850.
65. H. Rosenbrock, Some general implicit processes for the numerical solution of differential equations, *Comput. J.*, **5** (1963), 329–330.
66. Y. Sang, L. C. Miller, F. Blecha, Macrophage polarisation in virus-host interactions, *J. Clin. Cell. Immunol.*, **6** (2015), 311.
67. A. Sica, P. Larghi, A. Mancino, L. Rubino, C. Porta, M. G. Totaro, et al., Macrophage polarisation in tumour progression, *Seminars in Cancer Biology*, **18** (2008), 349–355.

68. I. Simon, N. van Rooijen, J. Rose, Vesicular stomatitis virus genomic RNA persists *in vivo* in the absence of viral replication, *J. Virol.*, **84** (2010), 3280–3286.

69. S. Sousa, R. Brion, M. Lintunen, P. Kronqvist, J. Sandholm, J. Mönkkönen, et al., Human breast cancer cells educate macrophages toward the M2 activation status, *Breast Cancer Res.*, **17** (2015), 101.

70. J. Sur, R. Allende, A. Doster, Vesicular stomatitis virus infection and neuropathogenesis in the murine model are associated with apoptosis, *Vet. Pathol.*, **40** (2003), 512–520.

71. T. Theodossiou, M. Ali, M. Grigalavicius, B. Grallert, P. Dillard, K. Schink, et al., Simultaneous defeat of MCF7 and MDA-MB-231 resistances by a hypericin PDT–tamoxifen hybrid therapy, *npj Breast Cancer*, **5** (2019), 13.

72. B. Vincenzi, M. Fioramonti, M. Iuliani, F. Pantano, G. Ribelli, D. Santini, et al., M1-polarized macrophages as predictor of poor response to trabectedin treatment in myxoid liposarcoma, *J. Clin. Oncol.*, **34** (2016), e22537–e22537.

73. S. Vinogradov, G. Warren, X. Wei, Macrophages associated with tumours as potential targets and therapeutic intermediates, *Nanomedicine*, **9** (2014), 695–707.

74. S. Waggoner, S. Reighard, I. Gyurova, S. Cranert, S. Mahl, E. Karmele, et al., Roles of natural killer cells in antiviral immunity, *Curr. Opin. Virol.*, **16** (2016), 15–23.

75. Y. Wang, T. Yang, Y. Ma, G. V. Halade, J. Zhang, M. L. Lindsey, et al., Mathematical modelling and stability analysis of macrophage activation in left ventricular remodelling post-myocardial infarction, *BMC Genomics*, **13** (2012), S21.

76. D. Wang, N. G. Naydenov, M. G. Dozmorov, J. E. Koblinski, A. I. Ivanov, Anillin regulates breast cancer cell migration, growth, and metastasis by non-canonical mechanisms involving control of cell stemness and differentiation, *Breast Cancer Res.*, **22** (2020), 3.

77. D. Wodarz, Computational modelling approaches to the dynamics of oncolytic viruses, *Wiley Interdiscip. Rev.: Syst. Biol. Med.*, **8** (2016), 242–252.

78. S. Yona, K. W. Kim, Y. Wolf, A. Mildner, D. Varol, M. Breker, et al., Fate mapping reveals origins and dynamics of monocytes and tissue macrophages under homeostasis, *Immunity*, **38** (2013), 79–91.

79. M. Zhang, Y. He, X. Sun, Q. Li, W. Wang, A. Zhao, et al., A high m1/m2 ratio of tumour-associated macrophages is associated with extended survival in ovarian cancer patients, *J. Ovarian Res.*, **7** (2014), 19.

80. Y. Zhu, A. Yongky, J. Yin, Growth of an RNA virus in single cells reveals a broad fitness distribution, *Virology*, **385** (2009), 39–46.

81. J. C. Zhuang, G. N. Wogan, Growth and viability of macrophages continuously stimulated to produce nitric oxide, *Proc. Natl. Acad. Sci. USA*, **94** (1997), 11875–11880.

Appendix A: Rescaled model (2.1)

To avoid numerical problems caused by some very large parameters (K_1, K_2) and some very small parameters (β_1, β_2), we decided to rescale the variables in system (2.1) as follows:

$$T_u^* = \frac{T_u}{K_1},\ T_i^* = \frac{T_i}{K_1},\ M_1^* = \frac{M_1}{K_2},\ M_{2u}^* = \frac{M_{2u}}{K_2},\ V^* = \frac{V}{V_{max}},$$

where V_{max} is the maximum possible VSV level that does not lead to neurotropism and neurovirulence (which has been observed rodents infected with VSV [7, 23, 70]). While normal experimental doses of VS range between $10^6 - 10^9$ [7], here we consider $V_{max} = 10^{11}$PFU.

$$\beta_1^* = \beta_1 V_{max}, \quad \beta_1^* = \beta_2 V_{max}, \quad b^* = \frac{b}{V_{max}} K_1, \quad c^* = \frac{c}{V_{max}} K_2, \quad a_2^{u*} = \frac{a_2^u K_1}{K_2},$$

$$a_1^{v*} = \frac{a_1^v}{K_2} V_{max}, \quad a_1^{i*} = \frac{a_1^i K_1}{K_2}, \quad a_1^{u*} = \frac{a_1^u K_1}{K_2}, \quad h_m^* = \frac{h_m}{K_2}, \quad h_u^* = \frac{h_u}{K_1}, \quad h_v^* = \frac{h_v}{V_{max}}.$$

We can drop the " $*$ " for simplicity. The rescaled model is similar to model (2.1), since we did not remove any variables/parameters; we only rescaled the variables/parameters (see also the 5^{th} column in Table 1).

Appendix B: Changing in model dynamics when assuming that infected tumour and macrophages cells can affect the carrying capacities

Here we investigate numerically the dynamics of model (2.1) when we assume that infected tumour cells and macrophages can also impact the carrying capacities. Thus Eqs (2.1a)–(2.1c) become:

$$\frac{dT_u}{dt} = rT_u\left(1 - \frac{T_u + g_1 T_i}{K_1}\right) - \beta_1 V T_u - d_u T_u \frac{M_1}{h_m + M_{2u}} + d_m T_u \frac{M_{2u}}{h_m + M_{2u}}, \tag{A.1a}$$

$$\frac{dM_1}{dt} = a_1^v V + a_1^i T_i + a_1^u T_u + p_{m1} M_1\left(1 - \frac{M_1 + M_{2u} + g_2 M_{2i}}{K_2}\right) - d_{e1} M_1 - M_1\left(r_{m1}^0 + r_{m1}^u \frac{T_u}{h_u + T_u}\right) + M_{2u}\left(r_{m2}^0 + r_{m2}^v \frac{V}{h_v + V}\right), \tag{A.1b}$$

$$\frac{dM_{2u}}{dt} = a_2^u T_u + p_{m2} M_{2u}\left(1 - \frac{M_1 + M_{2u} + g_2 M_{2i}}{K_2}\right) + M_1\left(r_{m1}^0 + r_{m1}^u \frac{T_u}{h_u + T_u}\right) - d_{e2} M_{2u} - M_{2u}\left(r_{m2}^0 + r_{m2}^v \frac{V}{h_v + V}\right) - \beta_2 V M_{2u}, \tag{A.1c}$$

In Figure 14 we show the baseline dynamics of model (A.1) for the baseline parameters listed in Table 1 when we consider $g_1 = g_2 = 0$ (the baseline case; cyan continuous curve); $g_1 = 1$ and $g_2 = 0$ (dotted black curve); $g_1 = 0$, and $g_2 = 1$ (the dashed green curve); $g_1 = 1$ and $g_2 = 1$ (the dash-dot curve). We see that there is no significant difference between the cases with $g_i = 0$ and $g_i = 1$, $i \in \{0, 1\}$. Therefore, for simplicity, we can work with the case $g_{1,2} = 0$; see model (2.1).

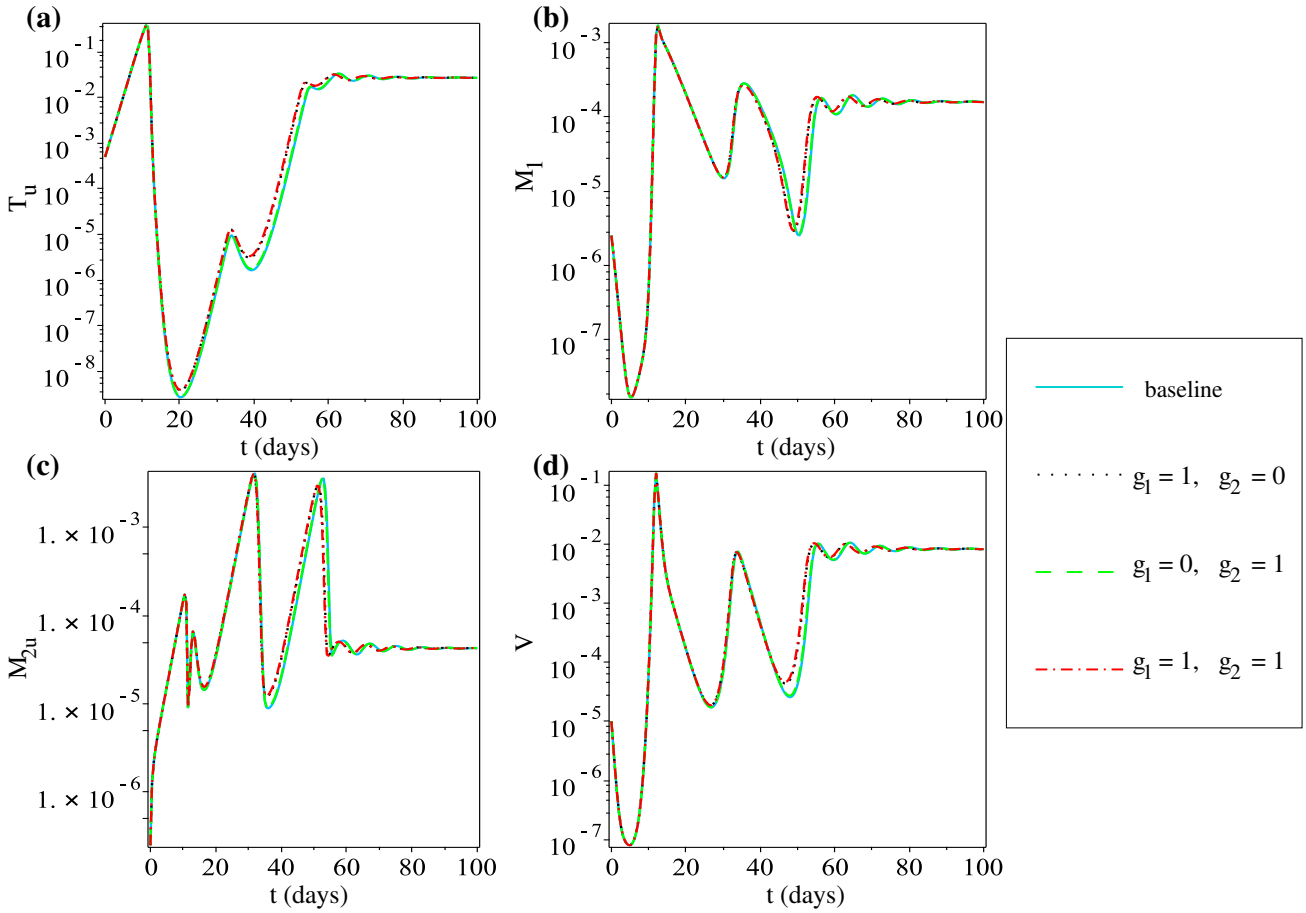

Figure 14. The dynamics of (a) tumour cells, (b) M1 cells, (c) M2 cells, and (d) virus particles for model (A.1) when we we assume that $g_1, g_2 \in \{0, 1\}$ (corresponding to the cases where infected tumour cells impact or not the carrying capacity K_1, and infected macrophages impact or not the carrying capacity K_2). The rest of parameter values are listed in Table (1).

Appendix C: Linear stability of steady states for model (2.1)

For the proof of Proposition 3 we use the Jacobian matrix associated with system (2.1a)–(2.1f). At a generic equilibrium point, this matrix is:

$$J(T_u^*, T_i^*, M_1^*, M_{2u}^*, M_{2i}^*, V^*) = \begin{bmatrix} b_{11} & b_{12} & b_{13} & b_{14} & b_{15} & b_{16} \\ b_{21} & b_{22} & b_{23} & b_{24} & b_{25} & b_{26} \\ b_{31} & b_{32} & b_{33} & b_{34} & b_{35} & b_{36} \\ b_{41} & b_{42} & b_{43} & b_{44} & b_{45} & b_{46} \\ b_{51} & b_{52} & b_{53} & b_{54} & b_{55} & b_{56} \\ b_{61} & b_{62} & b_{63} & b_{64} & b_{65} & b_{66} \end{bmatrix}, \tag{A.2}$$

with

$b_{11} = r\left(1 - \frac{T_u^*}{K_1}\right) - rT_u^* - \beta_1 V^* - \frac{d_u M_1^*}{hm + M_{2u}^*} + \frac{d_m M_{2u}^*}{hm + M_{2u}^*}$, $b_{12} = 0$, $b_{13} = -\frac{d_u T_u^*}{h_m + M_{2u}^*}$

$b_{14} = \frac{d_u T_u^* M_1^*}{(h_m + M_{2u}^*)^2} + \frac{d_m T_u^*}{h_m + M_{2u}^*}$, $b_{15} = 0$, $b_{16} = -\beta_1 T_u^*$, $b_{21} = \beta_1 V^*$, $b_{22} = -\delta_{i1} - \frac{d_i M_1^*}{h_m + M_{2u}^*}$,

$b_{23} = -\frac{d_i T_i^*}{h_m + M_{2u}^*}$, $b_{24} = \frac{d_i T_i^* M_1^*}{(h_m + M_{2u}^*)^2}$, $b_{25} = 0$, $b_{26} = \beta_1 T_u^*$, $b_{31} = a_1^u - M_1^* \left(\frac{r_{m1}^u}{h_u + T_u^*} - \frac{r_{m1}^u T_u^*}{(h_u + T_u)^2} \right)$,
$b_{32} = a_1^i$, $b_{33} = p_{m1} \left(1 - \frac{2M_1^* + M_{2u}^*}{K_2} \right) - r_{m1}^0 - \frac{r_{m1}^u T_u^*}{h_u + T_u^*} - d_{e1}$, $b_{34} = r_{m2}^0 - p_{m1} M_1^* + \frac{r_{m2}^v V^*}{1 + V^*}$, $b_{35} = 0$,
$b_{36} = a_1^v + M_{2u}^* \left(\frac{r_{m2}^v}{h_v + V^*} - \frac{r_{m2}^v V^*}{(h_v + V^*)^2} \right)$, $b_{41} = a_2^u + M_1^* \left(\frac{r_{m1}^u}{h_u + T_u^*} - \frac{r_{m1}^u T_u^*}{(h_u + T_u^*)^2} \right)$, $b_{42} = 0$, $b_{43} = r_{m1}^0 - p_{m2} M_{2u}^* + \frac{r_{m1}^u T_u^*}{h_u + T_u^*}$,
$b_{44} = p_{m2} \left(1 - \frac{M_1^* + 2M_{2u}^*}{K_2} \right) - r_{m2}^0 - \frac{r_{m2}^v V^*}{h_v + V^*} - d_{e2} - \beta_2 V^*$, $b_{45} = 0$, $b_{46} = -M_{2u}^* \left(\frac{r_{m2}^v}{h_v + V^*} - \frac{r_{m2}^v V^*}{(h_v + V^*)^2} \right) - \beta_2 M_{2u}^*$,
$b_{51} = 0$, $b_{52} = 0$, $b_{53} = 0$, $a_{54} = \beta_2 V^*$, $b_{55} = -\delta_{i2}$, $b_{56} = \beta_2 M_{2u}^*$, $b_{61} = 0$, $b_{62} = \delta_{i1} b$,
$b_{63} = -\frac{\delta_v V^*}{h_m + M_{2u}^*}$, $b_{64} = \frac{\delta_v V^* M_1^*}{(h_m + M_{2u}^*)^2}$, $b_{65} = c\, \delta_{i2}$, $b_{66} = -\omega - \frac{\delta_v M_1^*}{h_m + M_{2u}^*}$.

Appendix D: Stability of steady states shown in Figures 11 and 12

In the following we use the Jacobian matrix (A.2) to calculate the stability of the steady states TIVF, TVF, VF, TF and TIV shown in Figures 11 and 12 (for the specific parameter values used in these two figures).
Steady states and associated eigenvalues for the simulations shown in Figure 11:

- TIVF: $(0, 0, 0, 0, 0, 0)$
  Eigenvalues: $\lambda 1 = 0.62$, $\lambda 2 = 0.449$, $\lambda 3 = -0.311$, $\lambda 4 = -2$, $\lambda 5 = -0.399$, $\lambda 6 = -0.52$.
- TVF: $(0, 0, 0.001, 0.7867, 0, 0)$
  Eigenvalues:$\lambda 1 = 0.819$, $\lambda 2 = -0.449$, $\lambda 3 = -0.76$, $\lambda 4 = -3.525$, $\lambda 5 = -0.403$, $\lambda 6 = 1.005$.
- VF: $(1.3204, 0, 0.001, 0.7867, 0, 0)$
  Eigenvalues:$\lambda 1 = -0.819$, $\lambda 2 = -0.77$, $\lambda 3 = -0.449$, $\lambda 4 = -6.08$, $\lambda 5 = 3.65$, $\lambda 6 = -0.497$.
- TIV: $(0.1053, 0.0394, 0.0201, 0.058, 0.0455, 0.2916)$
  Eigenvalues:$\lambda 1 = -3.08$, $\lambda 2 = 0.105 + 0.68i$, $\lambda 3 = 0.105 - 0.68i$, $\lambda 4 = -0.64$, $\lambda 5 = -0.159$, $\lambda 6 = -0.41$.
- TF: $(0, 0, 0.0148, 0.1786, 0.1164, 0.242)$
  Eigenvalues:$\lambda 1 = -2.575$, $\lambda 2 = 0.398$, $\lambda 3 = -0.02 + 0.37i$, $\lambda 4 = -0.02 - 0.37i$, $\lambda 5 = -0.565$, $\lambda 6 = -0.436$.

Steady states and associated eigenvalues for the simulations shown in Figure 12:

- TIVF: $(0, 0, 0, 0, 0, 0)$
  Eigenvalues: $\lambda 1 = 0.62$, $\lambda 2 = 0.449$, $\lambda 3 = -0.311$, $\lambda 4 = -2$, $\lambda 5 = -0.399$, $\lambda 6 = -0.52$.
- TVF: $(0, 0, 0.001, 0.7867, 0, 0)$
  Eigenvalues:$\lambda 1 = 0.819$, $\lambda 2 = -0.449$, $\lambda 3 = -0.76$, $\lambda 4 = -3.215$, $\lambda 5 = -0.403$, $\lambda 6 = 0.69$.
- VF: $(1.3204, 0, 0.001, 0.7867, 0, 0)$
  Eigenvalues:$\lambda 1 = -0.819$, $\lambda 2 = -0.77$, $\lambda 3 = -0.449$, $\lambda 4 = -6.71$, $\lambda 5 = 4.298$, $\lambda 6 = -0.51$.
- TF: $(0, 0, 0.0166, 0.25, 0.14, 0.297)$
  Eigenvalues:$\lambda 1 = -2.569$, $\lambda 2 = 0.16$, $\lambda 3 = -0.04 + 0.346i$, $\lambda 4 = -0.04 - 0.346i$, $\lambda 5 = -0.53$, $\lambda 6 = -0.48$.
- TIV: $(0.02, 0.02, 0.02, 0.168, 0.11, 0.343)$
  Eigenvalues:$\lambda 1 = -2.66$, $\lambda 2 = 0.03 + 0.49i$, $\lambda 3 = 0.03 - 0.49i$, $\lambda 4 = -0.082$, $\lambda 5 = -0.58$, $\lambda 6 = -0.44$.

Appendix E: Global sensitivity and uncertainty analysis of M1 and M2 cells to model parameters

In Figures 15 and 16 we show the PRCC index for the two uninfected macrophage populations (as these tumour-infiltrating immune cells are assumed to have an impact on tumour dynamics). As in Figure 2, we randomly sampled each parameter 1000 times from the parameter ranges shown in Table 1. We simulated the dynamics of M1 and M2 cells for 14 days, with a time step of 1 day.
It is clear that the M1 cells are most sensitive to a_1^v (the activation rate of M1 cells in response to oncolytic viruses), h_u (half-saturation constant for tumour cells that trigger M1→M2 polarisation), p_{m1} (proliferation rate of M1 cells), r_{m2}^v (virus-induced M2→M1 re-polarisation), and ω (natural death rate of oncolytic viruses). The M2 cells are also sensitive to h_u and r_{m2}^v. In addition, they are somewhat sensitive to h_v (half-saturation constant for viruses that trigger M2→M1 re-polarisation).

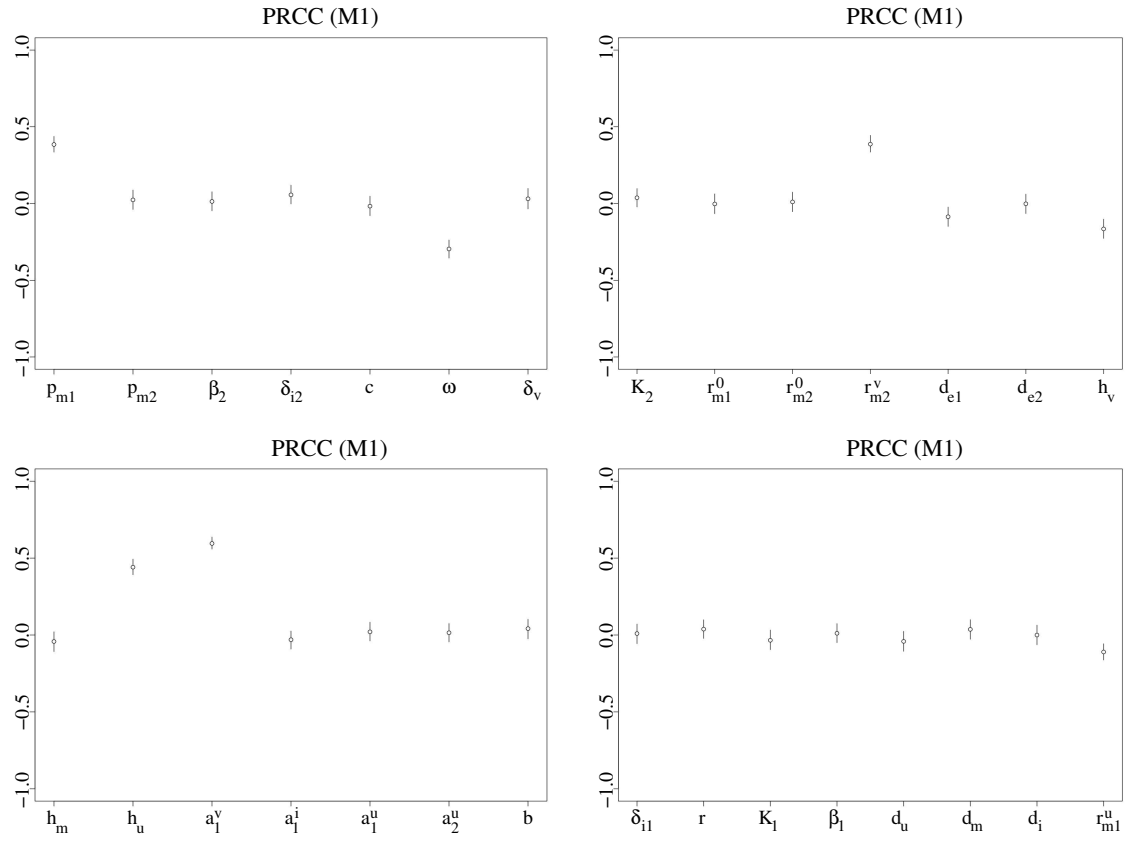

Figure 15. The effect of model parameters on M_1, as predicted by the LHS-PRCC analysis. The largest PRCC index (in absolute value) corresponds to the parameter with respect to which the model outcome (i.e., M_1) is most sensitive: p_{m1}, ω, r_{m2}^v, h_u, a_1^v.

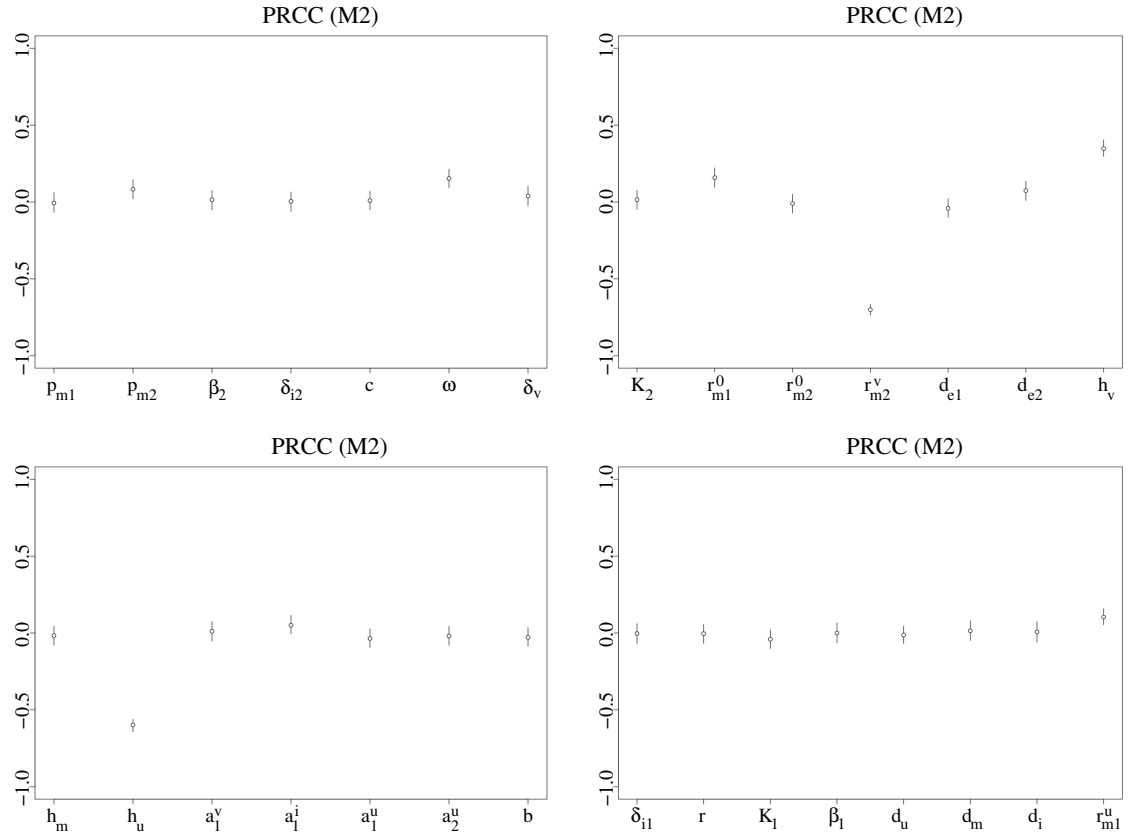

Figure 16. The effect of model parameters on M_2, as predicted by the LHS-PRCC analysis. The largest PRCC index in absolute value corresponds to the parameter with respect to which the model outcome (i.e., M_2) is most sensitive: r^v_{m2}, h_v, h_u.